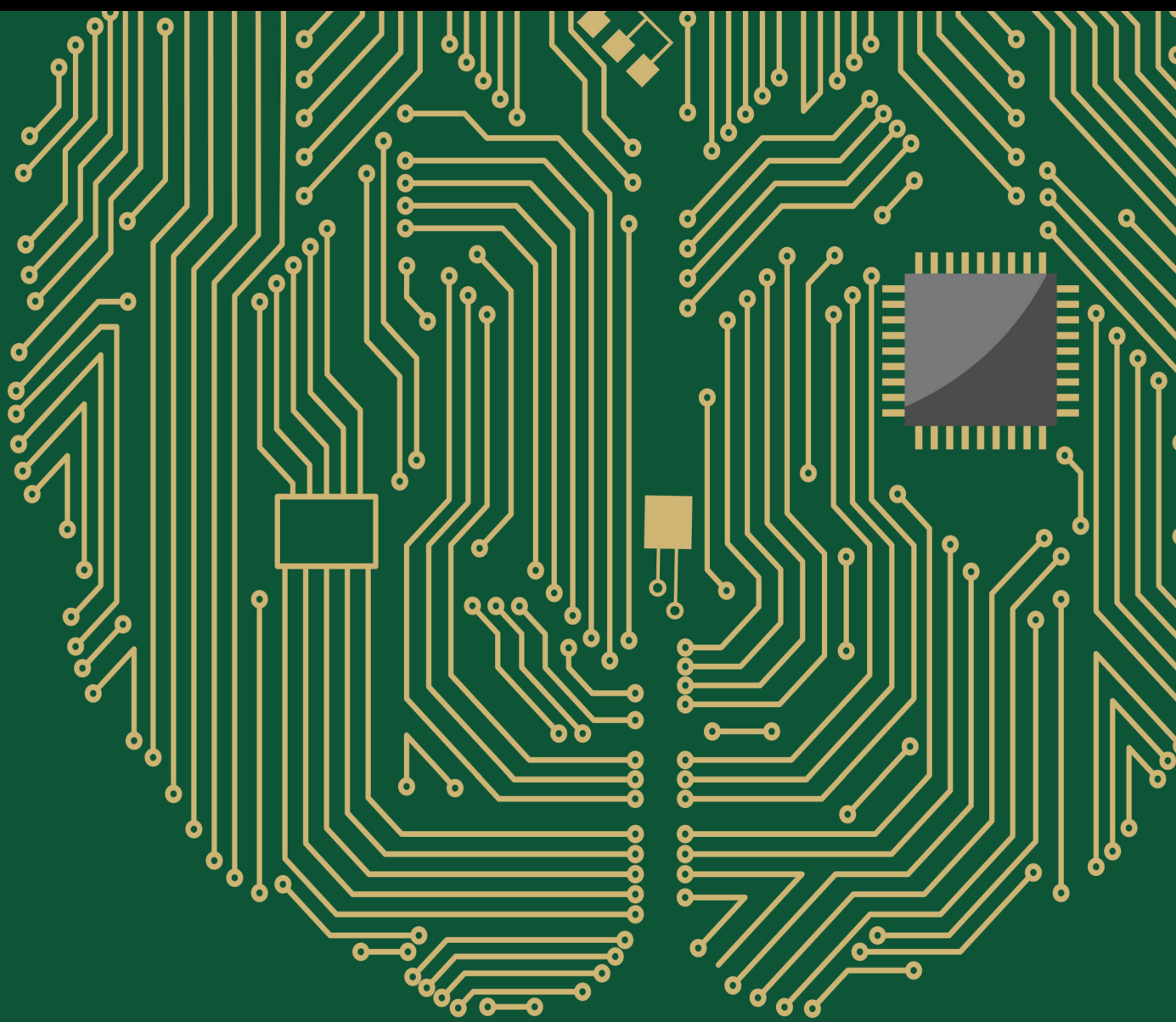


# Artificial Intelligence and Machine Learning for Alzheimer's Disease

Lead Guest Editor: Guangming Zhang

Guest Editors: Yun Shen and Jiesi Luo





---

# **Artificial Intelligence and Machine Learning for Alzheimer's Disease**

Computational Intelligence and Neuroscience

---

# **Artificial Intelligence and Machine Learning for Alzheimer's Disease**

Lead Guest Editor: Guangming Zhang

Guest Editors: Yun Shen and Jiesi Luo



---


Copyright © 2023 Hindawi Limited. All rights reserved.

This is a special issue published in "Computational Intelligence and Neuroscience." All articles are open access articles distributed under the Creative Commons Attribution License, which permits unrestricted use, distribution, and reproduction in any medium, provided the original work is properly cited.

# Chief Editor

Andrzej Cichocki, Poland

## Associate Editors

Arnaud Delorme, France  
Cheng-Jian Lin , Taiwan  
Saeid Sanei, United Kingdom

## Academic Editors

Mohamed Abd Elaziz , Egypt  
Tariq Ahanger , Saudi Arabia  
Muhammad Ahmad, Pakistan  
Ricardo Aler , Spain  
Nouman Ali, Pakistan  
Pietro Aricò , Italy  
Lerina Aversano , Italy  
Ümit Ağbulut , Turkey  
Najib Ben Aoun , Saudi Arabia  
Surbhi Bhatia , Saudi Arabia  
Daniele Bibbo , Italy  
Vince D. Calhoun , USA  
Francesco Camastra, Italy  
Zhicheng Cao, China  
Hubert Cecotti , USA  
Jyotir Moy Chatterjee , Nepal  
Rupesh Chikara, USA  
Marta Cimitile, Italy  
Silvia Conforto , Italy  
Paolo Crippa , Italy  
Christian W. Dawson, United Kingdom  
Carmen De Maio , Italy  
Thomas DeMarse , USA  
Maria Jose Del Jesus, Spain  
Arnaud Delorme , France  
Anastasios D. Doulamis, Greece  
António Dourado , Portugal  
Sheng Du , China  
Said El Kafhali , Morocco  
Mohammad Reza Feizi Derakhshi , Iran  
Quanxi Feng, China  
Zhong-kai Feng, China  
Steven L. Fernandes, USA  
Agostino Forestiero , Italy  
Piotr Franaszczuk , USA  
Thippa Reddy Gadekallu , India  
Paolo Gastaldo , Italy  
Samanwoy Ghosh-Dastidar, USA




Manuel Graña , Spain  
Alberto Guillén , Spain  
Gaurav Gupta, India  
Rodolfo E. Haber , Spain  
Usman Habib , Pakistan  
Anandakumar Haldorai , India  
José Alfredo Hernández-Pérez , Mexico  
Luis Javier Herrera , Spain  
Alexander Hošovský , Slovakia  
Etienne Hugues, USA  
Nadeem Iqbal , Pakistan  
Sajad Jafari, Iran  
Abdul Rehman Javed , Pakistan  
Jing Jin , China  
Li Jin, United Kingdom  
Kanak Kalita, India  
Ryotaro Kamimura , Japan  
Pasi A. Karjalainen , Finland  
Anitha Karthikeyan, Saint Vincent and the  
Grenadines  
Elpida Keravnou , Cyprus  
Asif Irshad Khan , Saudi Arabia  
Muhammad Adnan Khan , Republic of  
Korea  
Abbas Khosravi, Australia  
Tai-hoon Kim, Republic of Korea  
Li-Wei Ko , Taiwan  
Raşit Köker , Turkey  
Deepika Koundal , India  
Sunil Kumar , India  
Fabio La Foresta, Italy  
Kuruva Lakshmana , India  
Maciej Lawrynczuk , Poland  
Jianli Liu , China  
Giosuè Lo Bosco , Italy  
Andrea Loddo , Italy  
Kezhi Mao, Singapore  
Paolo Massobrio , Italy  
Gerard McKee, Nigeria  
Mohit Mittal , France  
Paulo Moura Oliveira , Portugal  
Debajyoti Mukhopadhyay , India  
Xin Ning , China  
Nasimul Noman , Australia  
Fivos Panetsos , Spain

Evgeniya Pankratova , Russia  
Rocío Pérez de Prado , Spain  
Francesco Pistolesi , Italy  
Alessandro Sebastian Podda , Italy  
David M Powers, Australia  
Radu-Emil Precup, Romania  
Lorenzo Putzu, Italy  
S P Raja, India  
Dr.Anand Singh Rajawat , India  
Simone Ranaldi , Italy  
Upaka Rathnayake, Sri Lanka  
Navid Razmjooy, Iran  
Carlo Ricciardi, Italy  
Jatinderkumar R. Saini , India  
Sandhya Samarasinghe , New Zealand  
Friedhelm Schwenker, Germany  
Mijanur Rahaman Seikh, India  
Tapan Senapati , China  
Mohammed Shuaib , Malaysia  
Kamran Siddique , USA  
Gaurav Singal, India  
Akansha Singh , India  
Chiranjibi Sitaula , Australia  
Neelakandan Subramani, India  
Le Sun, China  
Rawia Tahrir , Iraq  
Binhua Tang , China  
Carlos M. Travieso-González , Spain  
Vinh Truong Hoang , Vietnam  
Fath U Min Ullah , Republic of Korea  
Pablo Varona , Spain  
Roberto A. Vazquez , Mexico  
Mario Versaci, Italy  
Gennaro Vessio , Italy  
Ivan Volosyak , Germany  
Leyi Wei , China  
Jianghui Wen, China  
Lingwei Xu , China  
Cornelio Yáñez-Márquez, Mexico  
Zaher Mundher Yaseen, Iraq  
Yugen Yi , China  
Qiangqiang Yuan , China  
Miaolei Zhou , China  
Michal Zochowski, USA  
Rodolfo Zunino, Italy

## Contents

---

**Using CNN Saliency Maps and EEG Modulation Spectra for Improved and More Interpretable Machine Learning-Based Alzheimer's Disease Diagnosis**

Marilia Lopes , Raymundo Cassani , and Tiago H. Falk 

Research Article (17 pages), Article ID 3198066, Volume 2023 (2023)

**Increased Risk of Suicide among Cancer Survivors Who Developed a Second Malignant Neoplasm**

Huazhen Yang , Yuanyuan Qu , Yanan Shang , Chengshi Wang , Junren Wang , Donghao Lu , and Huan Song 

Research Article (11 pages), Article ID 2066133, Volume 2022 (2022)

## Research Article

# Using CNN Saliency Maps and EEG Modulation Spectra for Improved and More Interpretable Machine Learning-Based Alzheimer's Disease Diagnosis

Marilia Lopes <sup>1</sup>, Raymundo Cassani <sup>2</sup>, and Tiago H. Falk <sup>1</sup>

<sup>1</sup>*Institute National de la Recherche Scientifique (INRS-EMT), University of Quebec, Montreal, Canada*

<sup>2</sup>*McConnell Brain Imaging Centre, Montreal Neurological Institute, McGill University, Montreal, Canada*

Correspondence should be addressed to Marilia Lopes; [marilia.soares@inrs.ca](mailto:marilia.soares@inrs.ca)

Received 9 May 2022; Revised 15 September 2022; Accepted 11 January 2023; Published 8 February 2023

Academic Editor: Guangming Zhang

Copyright © 2023 Marilia Lopes et al. This is an open access article distributed under the Creative Commons Attribution License, which permits unrestricted use, distribution, and reproduction in any medium, provided the original work is properly cited.

Biomarkers based on resting-state electroencephalography (EEG) signals have emerged as a promising tool in the study of Alzheimer's disease (AD). Recently, a state-of-the-art biomarker was found based on visual inspection of power modulation spectrograms where three “patches” or regions from the modulation spectrogram were proposed and used for AD diagnostics. Here, we propose the use of deep neural networks, in particular convolutional neural networks (CNNs) combined with saliency maps, trained on power modulation spectrogram inputs to find optimal patches in a data-driven manner. Experiments are conducted on EEG data collected from fifty-four participants, including 20 healthy controls, 19 patients with mild AD, and 15 moderate-to-severe AD patients. Five classification tasks are explored, including the three-class problem, early-stage detection (control vs. mild-AD), and severity level detection (mild vs. moderate-to-severe). Experimental results show the proposed biomarkers outperform the state-of-the-art benchmark across all five tasks, as well as finding complementary modulation spectrogram regions not previously seen via visual inspection. Lastly, experiments are conducted on the proposed biomarkers to test their sensitivity to age, as this is a known confound in AD characterization. Across all five tasks, none of the proposed biomarkers showed a significant relationship with age, thus further highlighting their usefulness for automated AD diagnostics.

## 1. Introduction

Alzheimer's disease (AD) is a degenerative brain disease and the most common cause of dementia [1, 2]. AD progression leads to the loss of cognitive (e.g., memory, reasoning, and communication) and behavioral functions that will ultimately interfere with the individual's daily life. Diagnosing AD can be challenging, as the disease can initiate pathophysiological processes 20 years before any clinical symptoms appear [3, 4]. As such, improving early diagnostics has become a fundamental element in AD research and therapy [5], especially since there are currently no cures for AD [6–8]. While a definite diagnosis for AD can only be achieved through a postmortem structural examination of the brain, clinical diagnosis currently relies on the use of medical history and exams, such as the mini-mental state

examination (MMSE) [9] and the clinical dementia rating (CDR) [10]. Moreover, a handful of biomarkers have also been incorporated into the clinical diagnostic process, including structural neuroimaging (e.g., magnetic resonance imaging (MRI)-based measures of hippocampal volumes) [11, 12], blood and urine samples [13], cerebral spinal fluids (e.g., tau and beta-amyloid levels) [14], and genetic risk profiling [15]. More recently, there has also been a push to incorporate biomarkers extracted from electroencephalograms (EEG) into the diagnostic process [16].

Indeed, EEG has proven to be a useful tool in the study of AD, with several advantages over other neuroimaging modalities, including noninvasiveness, lower cost, the possibility to detect early synaptic dysfunction prior to symptoms arising, and the possibility to more easily track the course of the disease [17]. EEGs record from the scalp the



electrical field produced by the interaction of neurons. Most of the published works have relied on the analysis of resting-state EEG (rsEEG) in either eyes-open or eyes-closed conditions, thus making the data collection procedure more comfortable for elderly patients [18]. Over the years, several changes in the EEG have been reported as a function of AD, namely, slowing of the EEG, reduction in signal complexity, perturbations in interelectrode synchrony/coherence, and a neuromodulatory deficit [19], resulting from the reduction of neurotransmitters due to damage to neuro-pathways by the disease. More recently, machine learning tools applied to conventional EEG spectral features have started to show promising results for AD diagnosis (e.g., see [20–22]); in some cases, accuracy around 90% has been reported.

In regards to features, typically rsEEG-based AD studies extract diagnostic features from the five traditional EEG frequency subbands, namely, delta ( $\delta = 0.1\text{--}4\text{Hz}$ ), theta ( $\theta = 4\text{--}8\text{Hz}$ ), alpha ( $\alpha = 8\text{--}12\text{Hz}$ ), beta ( $\beta = 12\text{--}30\text{Hz}$ ), and gamma ( $\gamma > 30\text{Hz}$ ). The work in references [23, 24], in turn, proposed the measurement of the spectrotemporal dynamics of each of these subbands and showed that improved diagnostic accuracy could be achieved. The resultant 2-dimensional (frequency vs. frequency) power modulation spectrogram was shown to not only improve accuracy but to also be more robust to artifacts commonly observed with EEGs [25]. The use of these conventional frequency bands, however, may not be optimal for AD analysis, as they have been defined based on visual inspection of EEG signals in healthy subjects [26]. In fact, the work in references [27, 28] showed that nontraditional bands were better for AD diagnostics. Building on these insights, the work in reference [29] used visual inspection to find optimal power modulation spectrogram regions or “patches” that improved diagnostic accuracy relative to conventional measures widely used in AD characterization.

In this article, we build on the work of [29] and propose the use of a data-driven method in order to find the optimal modulation spectrogram patches for AD diagnostics, whereas in [29], visual inspection was used. Visual inspection can lead to the loss of discriminatory information and potential biases, as well as reduce the interpretation of the results. In particular, we propose the use of saliency maps obtained from a convolutional neural network (CNN) trained to detect AD. Saliency maps provide insights into which regions of the input image the CNN is focusing on to make its decisions [30] and could improve the interpretability of the obtained results. While the use of saliency maps has been explored for AD classification based on MRIs [31, 32], it has yet to be explored for EEG data. Given the modulation spectrogram 2-dimensional representation and its improved discrimination relative to the conventional spectrogram, it can be a prime candidate for a saliency map-based biomarker. Experiments described herein show the usefulness of the proposed method not only in detecting AD but also in predicting AD severity level. Finally, the measure is shown to not be affected by participant age, a common confounding factor in AD studies.

The remainder of this paper is organized as follows: Section 2 describes the materials and methods used in our

experiments. Section 3 presents the experimental results and discusses them in light of the existing literature, including study limitations. Lastly, conclusions are presented in Section.

## 2. Materials and Methods

*2.1. Participants.* We rely on EEG data collected from fifty-four participants recruited from the Behavioral and Cognitive Neurology Unit of the Department of Neurology and the Reference Center for Cognitive Disorders at the Hospital das Clínicas in São Paulo, Brazil. AD diagnosis and identification of severity level (mild-AD or moderate-to-severe AD) were performed by experienced neurologists according to NINCDS-ADRDA criteria [33] and classified based on the Brazilian version of the MMSE [34]. Ethics approval was obtained from the Research Ethics Office, and all participants consented to participate in the study. The data have been divided into three groups: (i) “N” consists of 20 healthy elderly controls, (ii) “AD1” corresponds to 19 mild-AD patients, and (iii) “AD2” to the 15 patients diagnosed with moderate-to-severe AD. In experiments where all AD patients are combined (i.e., AD1+AD2), this group will be termed “AD”. Table 1 shows participant demographic details, including MMSE scores.

Inclusion criteria for the N group included MMSE score  $\geq 25$  and CDR score = 0, as well as no indication of functional cognitive decline. The AD1 group inclusion criteria, in turn, included  $\text{MMSE} \leq 24$  and  $0.5 \leq \text{CDR} \leq 1$ ; whereas for the AD2 group, they included an  $\text{MMSE} \leq 20$  and CDR score = 2. An additional criterion used for the two AD groups was the presence of functional and cognitive decline over the previous 12 months based on detailed interviews with knowledgeable informants. Exclusion criteria included diabetes mellitus, kidney disease, thyroid disease, alcoholism, liver disease, lung disease, or vitamin B12 deficiency, as these conditions can also cause cognitive decline.

*2.2. EEG Acquisition and Preprocessing.* For the acquisition of EEG signals, twenty channels were used following the 10–20 international mounting system. EEG signals were recorded with 12 bit resolution and 200 Hz sampling frequency using BrainTech 3.0 instrumentation (EMSA Equipamentos Médicos INC., Brazil). In addition, electrode impedance was kept below 10 k $\Omega$  and attached bi-auricular (A1 and A2) electrodes were used as reference. A resting-state eyes-closed (rsEEG) protocol was followed, and data were recorded for at least eight minutes for each participant.

Based on insights from reference [25], raw EEG was preprocessed with a zero-phase FIR bandpass filter with a bandwidth 0.5–45 Hz, followed by processing with the wavelet-enhanced independent components analysis (wICA) step to remove eye movement and/or muscle artifacts [35, 36].

*2.3. Power Modulation Spectrogram.* The 2-dimensional power modulation spectrogram representation has been proposed to characterize spectrotemporal changes in the

TABLE 1: Participant demographic details.

Group identifiers	Subjects (female)	Age (years)	Education (years)	MMSE
N	20 (9)	68.0 ± 8.6	10.1 ± 5.5	28.5 ± 1.7
AD1	19 (11)	74.1 ± 5.5	5.6 ± 2.8	19.4 ± 5.3
AD2	15 (9)	75.0 ± 11.8	4.1 ± 3.8	12.8 ± 5.0

EEG due to AD (e.g., see [37]). The signal processing steps involved in the computation of the representation can be seen in Figure 1. First, the EEG time series  $x(t)$  is processed by a time-frequency mapping to generate the time-frequency representation  $X(t, f)$ . This mapping can be a short-time Fourier transform, for example, or a wavelet transform. In order to measure the temporal dynamics of each spectral bin, a second transformation is done on the time-frequency signal, now across the time dimension. This is achieved with a Fourier transform (FT) of the instantaneous power of each spectral bin, resulting in the power modulation spectrogram  $X(f, f_{\text{mod}})$ , i.e.,

$$X(f, f_{\text{mod}}) = \mathcal{F}_t\{|X(t, f)|^2\}, \quad (1)$$

where  $\mathcal{F}_t\{\cdot\}$  indicates the Fourier transform over the time dimension and  $f_{\text{mod}}$  indicates the modulation frequency dimension. The final result is a frequency-modulation frequency spectral representation that describes the second-order periodicities that would not be present in conventional spectral or time-frequency representations [38, 39].

In its original version, frequency bins in this 2-dimensional representation were grouped across the conventional and modulation frequency axes into the five traditional subbands, namely, delta, theta, alpha, beta, and gamma, and each frequency-modulation frequency bin was used as a feature for AD detection (e.g., see [23, 37]). More recently, the work in reference [29] showed that the use of the traditional bands was not optimal for the task at hand, and through visual inspection, three new regions were defined and proposed, termed “patches,” as shown in Figure 2. The modulation energy computed from these three patches, as well as their ratios, was proposed as new features for AD diagnosis and severity level prediction. Experimental results showed their superiority to the traditional band-grouping strategy, but suggested that some of the patches could be a result of normal aging. In this work, we build on these patches and propose a data-driven manner to explore if optimal patches can be found that are indicative of AD and not normal aging. Experiments rely on a  $45 \times 45$  power modulation spectrogram, where each bin corresponds to 1 Hz resolution.

**2.4. Convolutional Neural Networks.** Deep learning has emerged as a very powerful pattern analysis tool over the last decade. Increases in computational power have allowed for artificial deep neural networks (DNNs) with multiple hidden layers and billions of parameters to be trained within reasonable time frames. This increase in computational capacity has resulted in the emergence of a number of new deep neural network architectures, such as convolutional neural networks (CNNs), recurrent neural networks (RNNs), and

recursive neural networks (RvNNs), to name a few [40]. Here, we rely on CNNs and saliency maps to extract new biomarkers of AD from EEG modulation spectrograms; hence, a brief description of CNNs is given for the sake of completeness; more details can be found in [41–44].

While feed-forward DNNs multiply the inputs by optimized weights obtained during the training, CNNs include layers that perform convolutions, i.e., the dot product of the convolution kernel with the layer’s input matrix. The convolution kernel slides along the input matrix for the layer, thus generating a new feature map that contributes to the input of the subsequent layer. This is followed by other layers such as pooling layers, fully-connected layers, and normalization layers [45]. CNNs have resulted in state-of-the-art image recognition performance [46], as each convolution layer extracts specific features from the image, such as vertical and horizontal lines, color and shape, contrast, exposure variations, or image borders, to name a few. Using sequential convolution layers, each new feature map builds on the properties captured by the previous map. Depending on the number of layers used and the type of data used during training, CNNs may even learn features that take care of preprocessing, detection, and recognition, thus enabling end-to-end systems. When used for biomarker development, their use may also result in regions that could be more robust to EEG artifacts.

While many deep learning models are regarded as “black boxes,” providing limited insights on what parts of the input image are being used for discrimination, so-called saliency maps have been proposed to overcome this limitation. This method measures the spatial support of a particular class in each image via a heatmap. Saliency maps have been used for region-of-interest extraction [47], medical imaging [48, 49], robot vision [50], and audio-visual integration [51, 52], in addition to AD diagnosis based on MRI [32]. Saliency maps are obtained by computing the gradient of the output category in relation to the input image. In this way, the impact of how the value of the output category changes in relation to a small change in the pixels of the input image is observed. The highlighted regions in the resulting map indicate that they are important areas for the classification provided, where a small change in that pixel would change the classification relative to other pixels. In essence, saliency maps are constructed by back-projecting the information corresponding to the identified class, thus allowing us to visualize image regions that mostly affect prediction. Here, the keras-vis [53] toolkit was used to extract saliency maps.

It is hypothesized that using saliency maps with EEG power modulation spectrograms will allow for new biomarkers of AD to be developed in a data-driven manner and for comparisons with visually inspected regions to be made. Unlike simple images, however, EEGs are extracted across

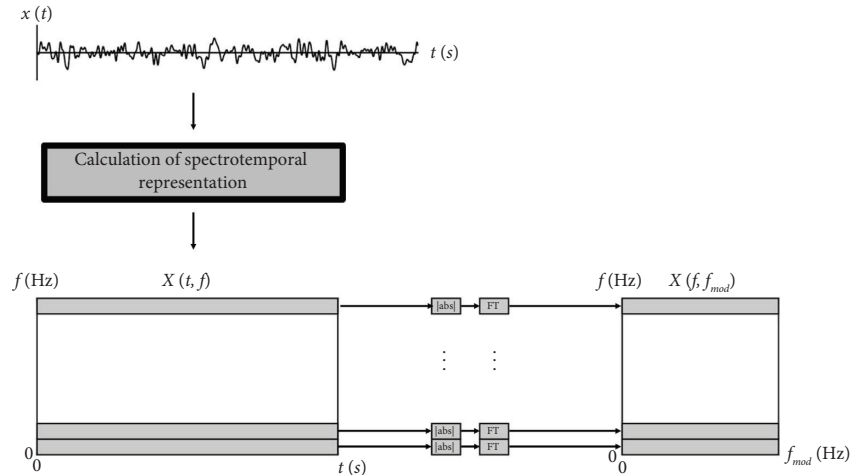


FIGURE 1: Signal processing steps for the computation of the EEG power modulation spectrogram. (Image adapted from [29]).

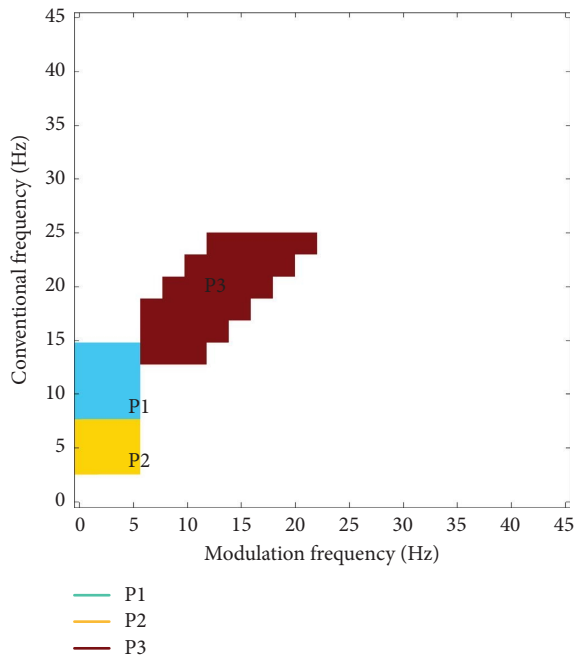


FIGURE 2: Three modulation spectrogram patches proposed in [29].

multiple channels, each generating its own image-like modulation spectrogram. As information from multiple channels is taken into account during classification, 20 different saliency maps, one for each EEG channel can be generated. While each of these maps could be used separately, here, for simplicity, we take their overall average and use the aggregated map for analysis; use of individual channel maps is left for a future study. In our experiments, a CNN with two convolution layers was used, having as input a tensor of  $45 \times 45 \times 20$  dimensionality. The kernel size is equal to  $3 \times 3$  and a dropout rate of 85% was used. ReLU activation functions were used for the convolution layers. In the fully-connected layers, in turn, LeakyReLU was used as an activation function. A total of three fully-connected layers were used, including the last classification layer. Hyper-

parameter tuning was performed, and Table 2 presents the tested parameters and final values used.

**2.5. Proposed Method.** Figure 3 depicts the block diagram of the proposed method. First, EEG signals are segmented and transformed to the power modulation spectrogram domain which is then z-normalized. Segments of 8-second duration with 1-second overlap are taken; a minimum of 460 segments are available per subject. CNNs are then trained on five different classification tasks, namely, Task 1 (T1):  $N$  vs. AD1 vs. AD2 (multi-class discrimination); Task 2 (T2):  $N$  vs. AD (AD diagnosis); Task 3 (T3):  $N$  vs. AD1 (early AD detection); Task 4 (T4): AD1 vs. AD2 (AD progression); and Task 5 (T5):  $N$  vs. AD2 (late-stage AD detection). Saliency maps are then extracted for each of the five tasks to indicate regions of importance for each task. To allow for comparisons with the three visually obtained regions [29], a clustering algorithm is applied on the saliency map “islands” to obtain new optimal patches. These patches are then used for classification. In the subsections to follow, more details about the clustering method and final classification steps are given. Algorithm 1 shows an overview of the processing steps involved in the feature extraction and train/testing stages of the proposed method.

**2.6. Saliency Map Clustering.** After the CNNs are trained, saliency maps are extracted from the last dense layer. Saliency maps from each training input are obtained and averaged over all training samples to obtain one final map. Here, we are interested in using the maps to find optimal regions in the modulation spectrogram for new biomarker development. To this end, we use thresholding and clustering to find the optimal number of patches, in a data-driven manner, for the particular task at hand. To find the optimal clusters per task for this final map, we propose to first take the difference between the average modulation spectrograms of the two groups in a given classification task and use the saliency map as a mask to be applied to this differential spectrogram. When clustering, two parameters

TABLE 2: CNN hyper-parameter tuning details.

Hyper-parameters	Range explored	Chosen
Kernel_size	(3.3), (5.5), (7.7), (9.9)	(3,3)
Regularizers.l2	( $1e-2$ ), ( $1e-4$ )	( $1e-2$ )
Dropout	(65%, 75%, 85%, 90%)	85%
Optimizer	Adam, Nadam, Adagrad, Adamax	Nadam
Learning rate	(0.01, 0.001, 0.0001)	0.0001
Batch_size	4, 8, 32, 64	4
Epochs	20, 30, 40, 50	50

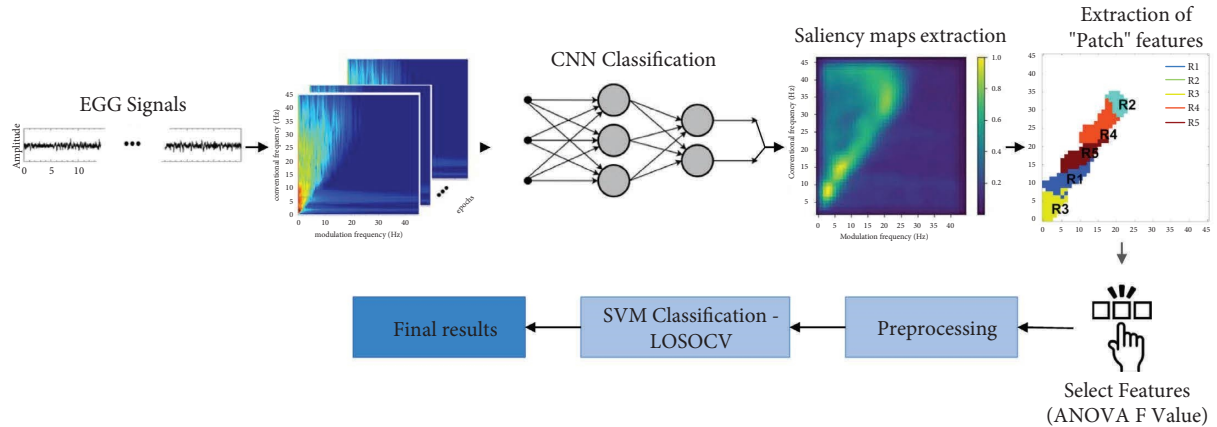
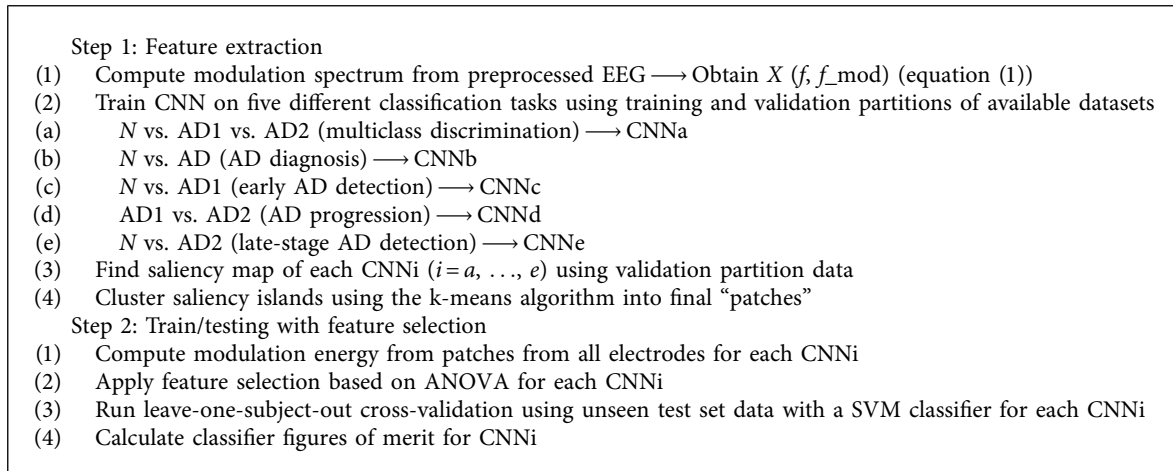


FIGURE 3: Overview of the proposed system architecture.



ALGORITHM 1: Summary of methodology steps.

are explored via grid search, namely, the saliency value threshold and the number of clusters. Threshold values from 80–96% were explored, with a hop of 2% and 3–5 clusters were tested. We selected three as the minimum to coincide with the patches proposed in [54] and five to strike a balance with feature dimensionality. Clustering was performed via the k-means algorithm in MATLAB.

Four distinct masking approaches are tested to explore their impact on overall accuracy. They vary based on which task the saliency map was obtained from, e.g., more generic, as in Task 2, to more specific, as in Task 3. These four different experiments are detailed as follows:

- (i) Experiment 1: This experiment takes the generic  $N$  vs. AD task and uses the saliency map obtained from the three-class task  $N$  vs. AD1 vs. AD2 as a mask.
- (ii) Experiment 2: This second experiment is a bit more tuned to the task at hand as it considers individual subclasses directly, while still using the most generic saliency map. In particular, the difference signal is taken for each binary task, namely,  $N$  vs. AD1,  $N$  vs. AD2, and AD1 vs. AD2. The same saliency map as Experiment 1 is used.
- (iii) Experiment 3: This is the most specialized of the experiments as the saliency maps corresponding to

each differential modulation spectrograms are used to find the optimal clusters. For example, saliency maps found for the  $N$  vs. AD1,  $N$  vs. AD2, and AD1 vs. AD2 tasks are used with differential spectrograms obtained from  $N$  vs. AD1,  $N$  vs. AD2, and AD1 vs. AD2 classes, respectively.

- (iv) Experiment 4: This experiment builds on Experiment 1 and takes the  $N$  vs. AD task and uses the saliency map obtained from the same  $N$  vs. AD mask, which can be seen as the most generic.

**2.7. Biomarker Selection and AD Diagnosis.** Once the optimal number of clusters is found, these regions will become candidate patches for each of the five tasks. As in [29], the modulation spectrum power  $R_i$  in patch/cluster  $i$  is computed as follows:

$$R_i = \iint_{RG_i} |X(f, f_{\text{mod}})|^2 df df_{\text{mod}}, \quad (2)$$

where  $RG_i$  corresponds to the new patch found by cluster  $i$ . As in [54], the power ratios between different patches are also treated as features and these are computed across all 20 channels.

As can be seen, the number of candidate features/biomarkers can quickly grow with an increasing number of channels and regions, causing potential curse-of-dimensionality issues with the downstream classification tasks. As such, feature selection is needed to reduce the final number of features to a reasonable number. Previous EEG-based works have relied on 24 input features (e.g., see [23, 25]), and we follow this procedure to allow for fair comparisons with prior works. We use 25% of the training set (described in the next subsection) to find the best 24 features using an ANOVA  $F$ -value metric computed between each feature and class label.

Previous works have relied on a support vector machine (SVM) classifier to map patch features to a final diagnostic decision. For consistency, we also use an SVM for final AD classification, thus allowing for a more fair comparison with previous work. This also assures that the performance gains achieved are a result of the improved biomarkers and not of an improved classifier (e.g., a CNN itself). SVMs use kernels to map data from two classes into a higher dimension in which a hyperplane can be used to separate the two different classes by a certain margin [55]. Different kernels provide different properties and allow for more complex class partitions to be found. Here, a radial basis function (RBF) kernel with gamma  $\gamma = 1/24$ , where 24 is the number of features, and  $C = 1$  are used as hyper-parameters and tuning is not performed to gauge the benefits of the features themselves, and not on the classifier. Prior to classification, the top-24 new biomarkers are normalized between  $[-1, 1]$ . Final testing follows a leave-one-subject-out (LOSO) plus bootstrapping procedure using the disjoint test set described below. With the LOSO-plus-bootstrapping setup, for each subject, the classifier is trained with data from  $N - 1$  subjects that are randomly sampled and repeated ten times.

**2.8. Testing Setup.** The available dataset has to be split to allow for CNN training for biomarker selection as well as for SVM training for final classification. As such, the available data needs to be partitioned in such a way that data leakage does not occur into the final test set. To this end, the data partitioning scheme illustrated in Figure 4 is performed to avoid any data leakage into the disjoint training, validation, and test sets. First, the 460 segments are partitioned into five parts, each with 92 segments. Since the segments are obtained with a 7-second overlap, the last 7 segments of each part are discarded, to avoid information leakage between folds (see Figure 4(a)). Each of the five parts is comprised of 85 segments, for each of the 54 subjects (Figure 4(b)). Finally, a time-dimension shuffle was made to avoid any ordering effects on the data. From the shuffled data, 1/5 of the data was set aside for validation, 1/5 for testing, and 3/5 for training (Figure 4(c)).

**2.9. Figures-of-Merit and Benchmark Method.** We use accuracy and  $F1$ -score as figures-of-merit to gauge the performance of the proposed method and compare against the visual-inspection-based biomarkers from [29]. Accuracy represents the ratio of correct predictions to total predictions, i.e.,

$$\text{Accuracy} = \frac{\text{TP} + \text{TN}}{\text{TP} + \text{TN} + \text{FP} + \text{FN}}, \quad (3)$$

where TP stands for true positive (target label is correctly predicted), TN for true negative (nontarget label predicted correctly as nontarget), FP for false positive (nontarget label predicted as target), and FN for false negative (target label erroneously predicted as nontarget).

In turn,  $F1$ -score is given by the weighted average between recall and precision, namely,

$$F1 = \frac{2 * \text{precision} * \text{recall}}{\text{precision} + \text{recall}}. \quad (4)$$

$F1$ -scores are useful for unbalanced datasets, such as the one used here. For completeness, precision identifies how accurately the model predicted the positive classes, i.e.,

$$\text{Precision} = \frac{\text{TP}}{\text{TP} + \text{FP}}, \quad (5)$$

where recall measures the ratio of the number of true positive events to the sum of true positive and false negative events, i.e.,

$$\text{Recall} = \frac{\text{TP}}{\text{TP} + \text{FN}}. \quad (6)$$

As for the benchmark, we use the state-of-the-art system described in [29] for comparisons.

**2.10. Age-Related Confounds.** Age is a known confounding factor and risk factor for AD [56, 57]. Since the healthy and patient populations in our dataset are not age-matched, we need to be careful not to propose features that are correlates of normal neural deterioration due to aging (e.g., see

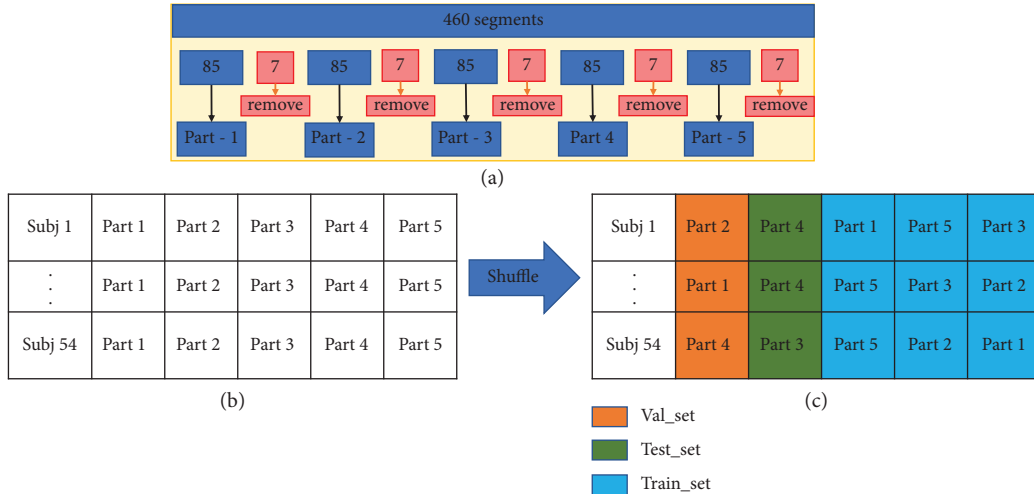


FIGURE 4: Steps to perform database partitioning to avoid information leakage. (a) First, 460 segments per subject are split into 5 parts of 92 segments. The last seven are discarded to avoid data leakage. (b) Disjoint parts are then combined per subject. (c) Lastly, temporal shuffle is done to avoid ordering effects. 1/5, 1/5, and 3/5 of the shuffled data are partitioned into validation, testing, and training subsets.

[58, 59]), but instead, related to neurodegeneration due to the disease. First, we explore how well the top-24 features can be used to predict age via a linear regression. To test if the top-selected features carry age-related information, we compare them against a random age prediction regressor. With this random linear regressor, we shuffle the age of participants in a random manner. For this task, we combine all the three dataset partitions and split them into train/test using 75% and 25% of the data, respectively. This partition is run 100 times, and the average root mean square error (between true and predicted age) and standard deviations are reported. To assure that the differences with the random regressor are not significant, a  $t$ -test is performed with a 99% confidence level ( $p > 0.01$ ); the Python statistical package `sciPy.stats` was used for this test.

### 3. Results and Discussion

**3.1. CNN Accuracy.** First, we explore how well the CNN is behaving on the validation set in order to gauge the effectiveness of the obtained saliency maps for downstream AD detection on the unseen test set. Table 3 reports the results obtained for each of the five classification tasks. We use only accuracy (Acc) and the  $F1$ -score for this analysis. Overall, the  $N$  vs. AD2 (T5) task resulted in the highest accuracy and  $F1$  score. This is expected, as the neural changes with moderate-to-severe AD are likely to be the greatest compared to healthy EEG, thus making it easier for the CNN to distinguish them. The accuracies obtained are in line with those reported previously for manually-selected clean EEG segments (e.g., see [23]), hence providing confidence on the potential of the CNN to find discriminatory features for AD classification, thus validating the use of the saliency maps for feature extraction and potentially artifact rejection.

**3.2. Saliency Maps.** With the CNN approach validated, we proceed to investigate the saliency maps generated from the

EEG channels. While each individual channel map could be used for channel-specific feature generation, here, for simplicity, we explore the use of only one general mask for all channels. As such, the average map is used. Figure 5 depicts the average map found for each of the five tasks. At a first glance, similar regions to the patches reported in reference [29] (shown in Figure 2) are seen, but with additional regions also showing importance. Next, we explore the best threshold and number of clusters for each of the four experiments tested.

**3.3. Saliency Map Clustering for Patch Detection.** Table 4 shows the best thresholds (Th) and number of clusters (C) found for each of the four experiments; henceforth, these combinations are used. The optimal patch regions found based on these parameters can be seen in Figures 6 and 7 for Experiment 1 and Experiment 4, respectively. The plots of the other two experiments are omitted for brevity, but similar regions were found. In each subfigure of these plots, the  $x$ -axis corresponds to modulation frequency, the  $y$ -axis to conventional frequency, the left-most plot shows the patches found with the optimal threshold, and the right-most plot shows the optimal clusters found. In each image, the found clusters/regions for each task are labelled as “ $R_i$ .” It is important to emphasize that each task achieved different regions of importance, hence, e.g.,  $R_1$  from Task 1 may differ from  $R_1$  from Task 2. As such, when listing the rank of top features in tables to follow, we use a subscript from 1–5 to remind the reader that the region listed is related to its corresponding counterpart seen in Figures 6 and 7.

As can be seen, the patches found using Experiment 1 settings resemble closer those found via visual inspection in reference [29], especially P2 and P3 seen in Figure 2. Other than the  $N$  vs. AD1 task, the obtained regions look fairly alike for all tasks. One region not used before but that was shown to be important in this data-driven analysis method corresponds to patches in lower frequencies, below 5 Hz (delta

TABLE 3: CNN accuracy on the validation set for the five tasks.

Tasks	Acc (%)	F1 (%)
T1	90.5	90.5
T2	87.3	84.6
T3	91.4	91.0
T4	92.5	91.4
T5	93.0	91.6

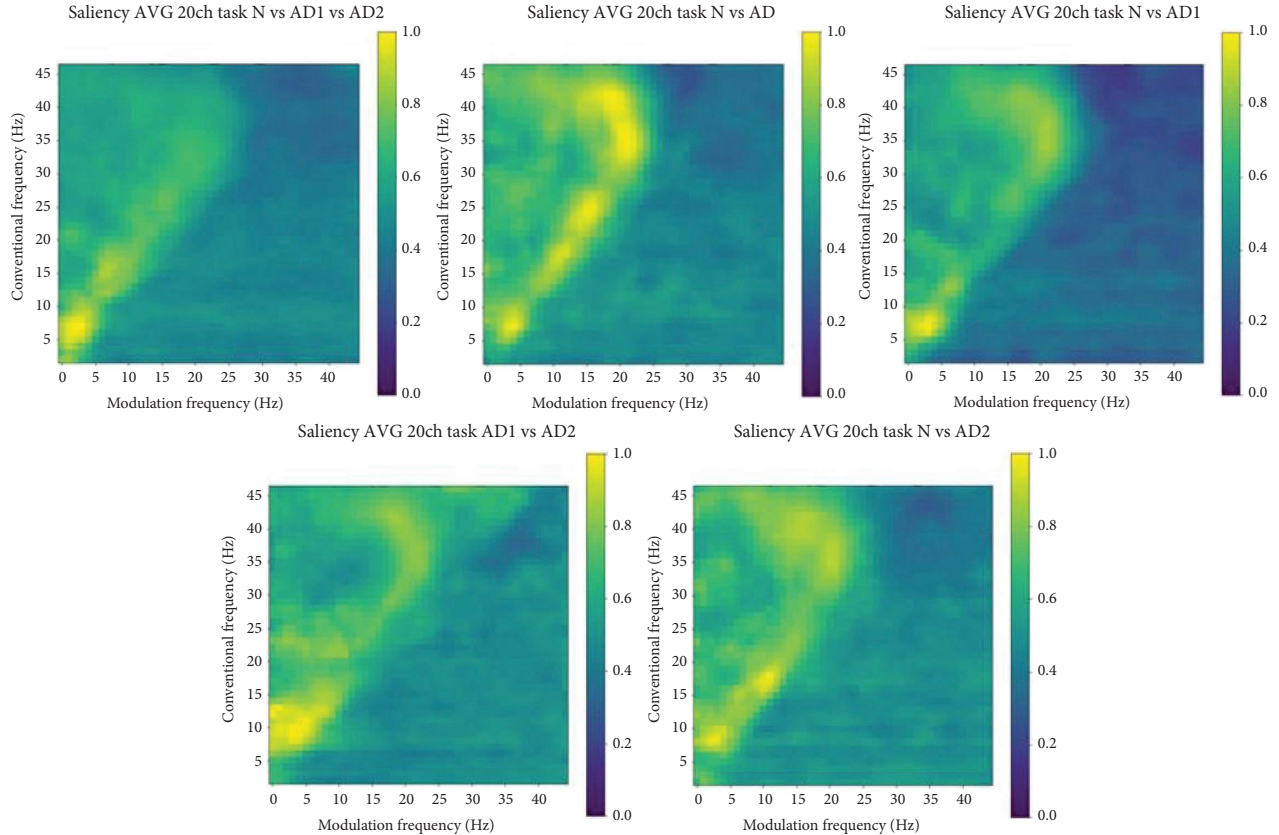


FIGURE 5: Average saliency map for each of the five tasks.

and low theta), corroborating some earlier findings from reference [23]. Experiment 4 settings, in turn, showed similar regions to those obtained from visual inspection but also included across all tasks important information extracted from higher frequencies (around the beta and gamma frequency ranges), a finding not seen previously in modulation spectral studies.

**3.4. Feature Importance.** The optimal patches for each classification task have now been found and they serve as masks for biomarker extraction from each EEG channel. To reduce the number of features being used by the SVM classifier, feature ranking is performed and only the top-24 features are kept. Table 5 lists the top features for each of the five tasks for the Experiment 1 setting. The notation RXoRY is used to indicate the feature corresponding to the ratio of the modulation power in patch RX to the modulation power in patch RY. Subscripts 1–5 indicate that the regions are those corresponding to Tasks 1–5. It can also be seen that for

the majority of the tasks, frontal region electrodes stood out. Interestingly, as reported in reference [25], frontal regions are usually discarded with EEG analysis relying on visual inspection of EEGs, as these areas are often contaminated by eye movement artifacts. Our findings suggest that such important regions may be again incorporated into EEG analysis by utilizing automated artifact removal algorithms, such as wICA, and features that could be inherently more robust to artifacts. For the AD1 vs. AD2 task, most features belong to the frontal and central electrodes, a region known to be affected by the progression of AD [60], likely due to the expansion of the atrophy into the superior parietal and frontal cortex [61]. For the *N* vs. AD and *N* vs. AD1 tasks, in turn, features extracted from the temporal brain region stood out, corroborating studies showing atrophy in cortical regions in the temporal regions [62]. In particular, in the *N* vs. AD1 task, temporal and frontal brain regions stood out; such fronto-temporal regions have been used for early AD diagnosis in the past [63].

TABLE 4: Best combination of threshold (Th) and number of clusters (C) for each of the four experiments.

Tasks	Exp. 1		Exp. 2		Exp. 3		Exp. 4	
	Th (%)	C	Th (%)	C	Th (%)	C	Th (%)	C
T1	92	3	92	3	92	3	92	3
T2	96	4	96	4	96	5	96	5
T3	86	3	84	4	92	4	96	3
T4	94	5	86	5	82	4	86	4
T5	96	3	92	4	94	3	90	4

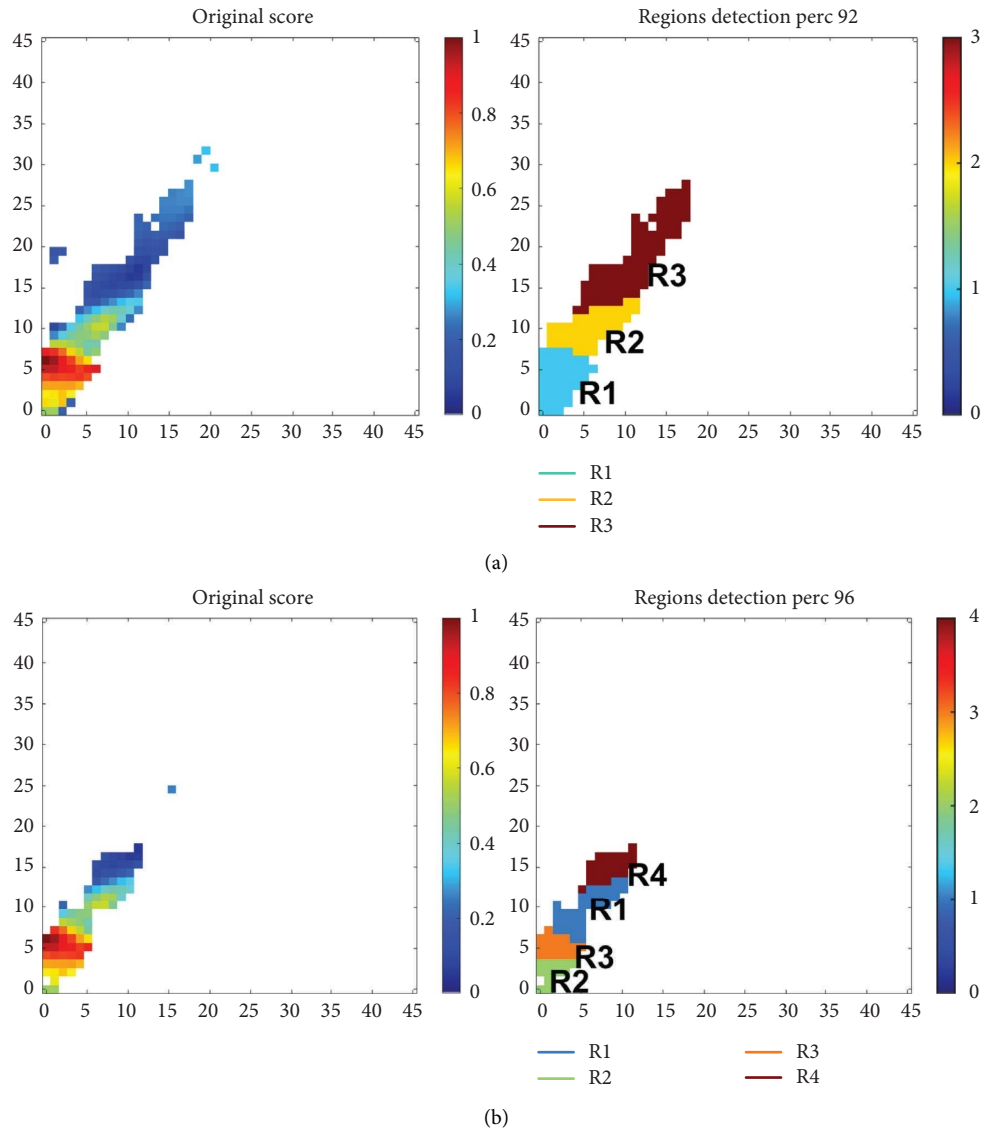


FIGURE 6: Continued.



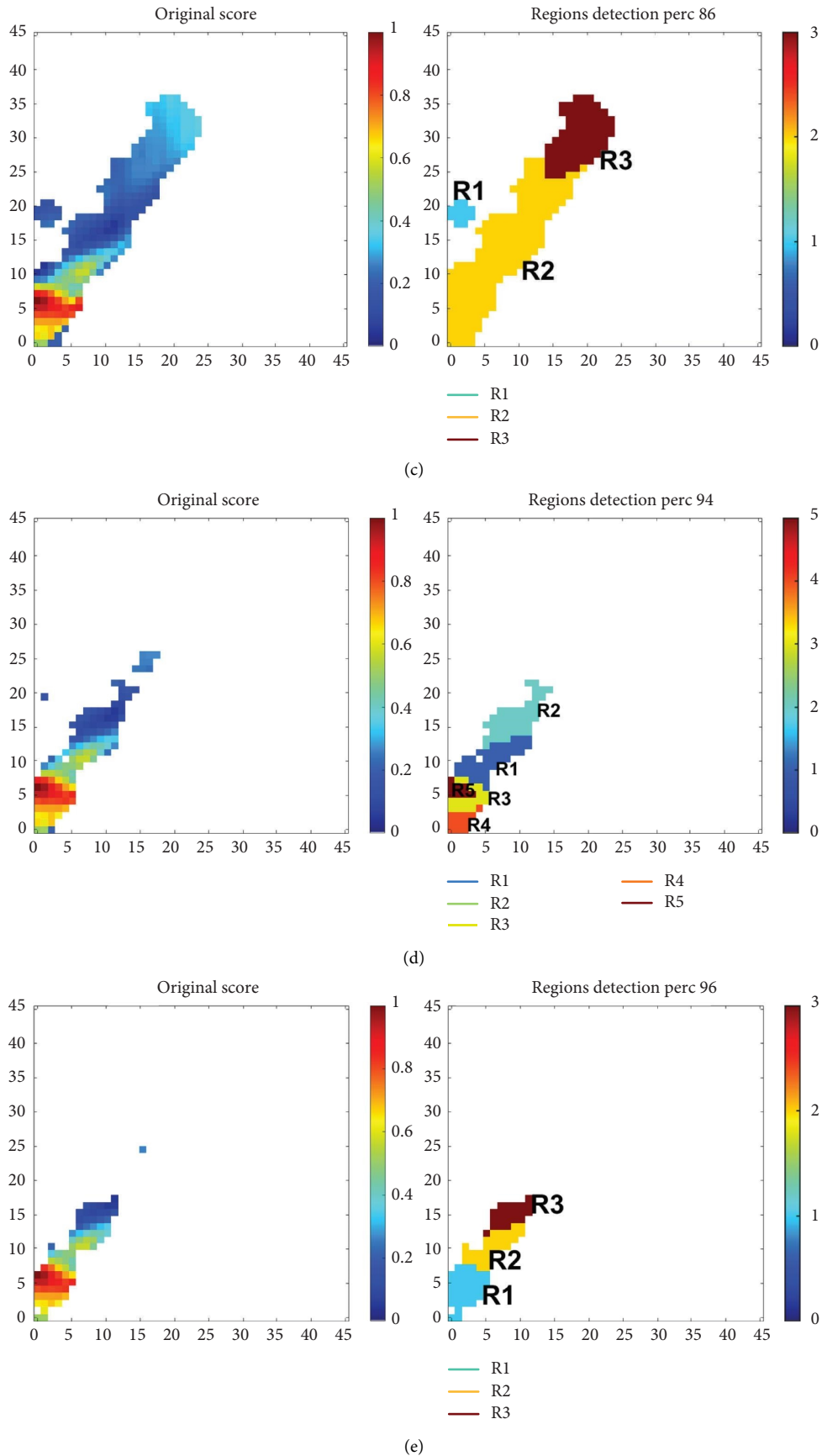
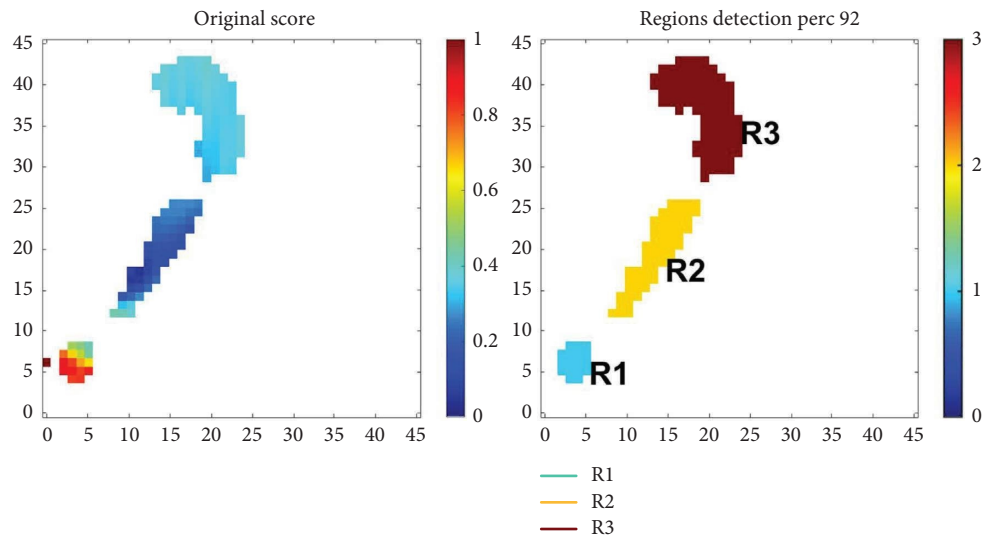
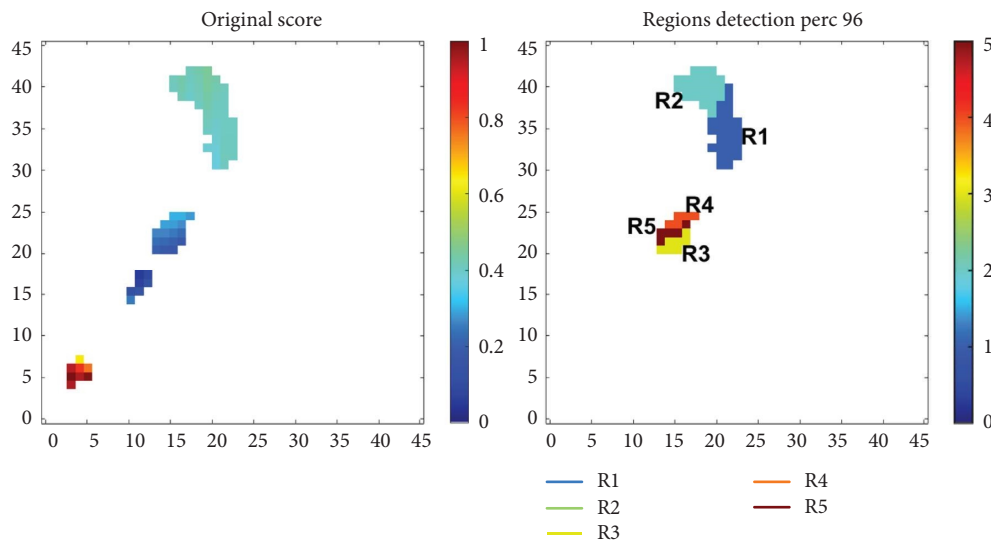


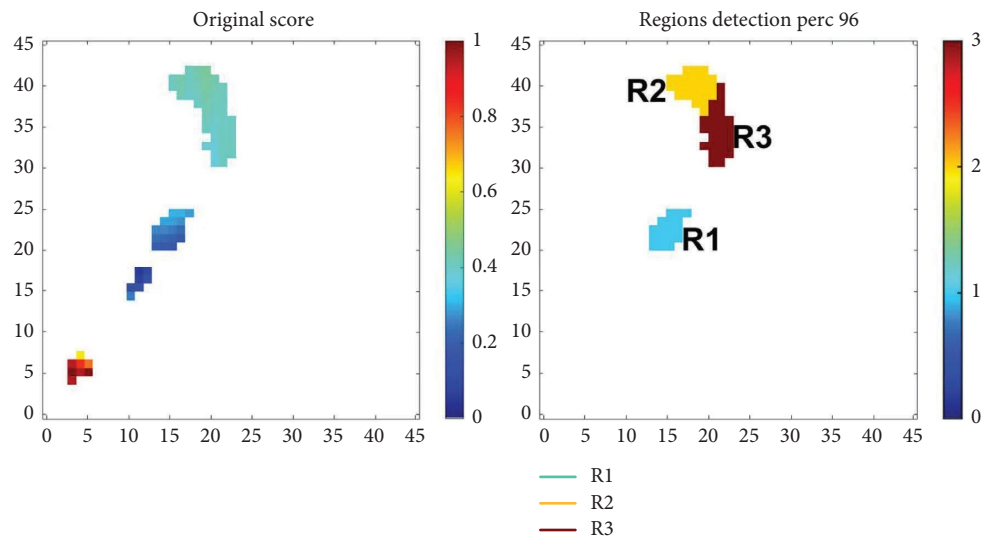
FIGURE 6: Optimal regions and clusters found for each of the five tasks using experiment 1 settings. In each subplot, the y-axis corresponds to conventional frequency (unit: Hz) and the x-axis to modulation frequency (unit: Hz). (a) *N* vs. AD1 vs. AD2, (b) *N* vs. AD, (c) *N* vs. AD1, (d) AD1 vs. AD2, and (e) *N* vs. AD2.



(a)



(b)



(c)

FIGURE 7: Continued.

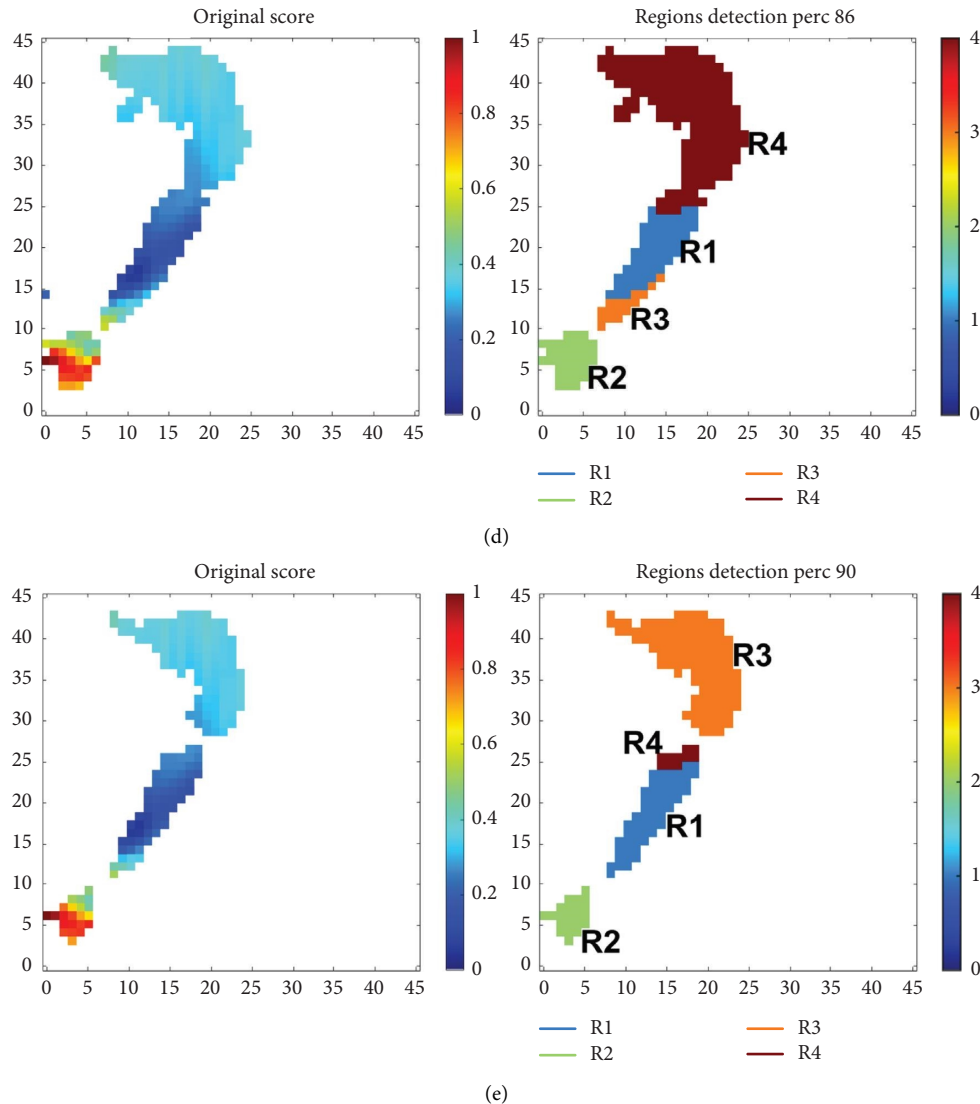


FIGURE 7: Optimal regions and clusters found for each of the five tasks on the experiment 4 settings. In each subplot, the  $y$ -axis corresponds to conventional frequency (unit: Hz) and the  $x$ -axis to modulation frequency (unit: Hz). (a)  $N$  vs. AD1 vs. AD2, (b)  $N$  vs. AD, (c)  $N$  vs. AD1, (d) AD1 vs. AD2, and (e)  $N$  vs. AD2.

As for the Experiment 4 setting, Table 6 shows the top-24 features selected. Unlike the Experiment 1 settings, high-frequency range features (both in conventional and modulation frequency domains) appear in the top-5 features for three of the five tasks, namely,  $N$  vs. AD,  $N$  vs. AD1, and AD1 vs. AD2. This suggests that such frequency ranges could be useful for early diagnosis and AD progression assessment, hence, providing new insights not previously achieved via visual inspection. Some research has shown the importance of gamma band activity in AD [64], though this region is often corrupted by muscle artifacts. The findings obtained here suggest that the temporal dynamics of the beta and gamma bands may provide some discriminatory information and that a more generic mask may capture the dynamics of a band that is typically discarded due to artifacts, hence further emphasizing the robustness of the new biomarkers. In addition, some of the regions found belong to the beta-m-

alpha and gamma-m-alpha frequencies. These frequencies have been shown in [65] to correlate with cerebral hemodynamics information conveyed by functional near-infrared spectroscopy in regions related to impaired blood flow in AD [66, 67], thus providing some additional interpretability to the selected biomarkers.

With these settings, it can be seen that most of the features were derived from electrodes over the temporal, parietal, and occipital regions, thus in agreement with [62]. An occipital brain region was most important for two of the five tasks ( $N$  vs. AD and  $N$  vs. AD1) and was the second most important region in the AD1 vs. AD2 task, hence corroborating classical findings from reference [68]. Unlike these classical studies, however, where occipital changes were found mostly in lower frequency ranges, here we observe them to be extracted from higher ranges around beta conventional frequency and gamma modulation

TABLE 5: Top 24 features selected using the experiment 1 settings.

Rankings	<i>N</i> vs. AD1 vs. AD2	<i>N</i> vs. AD	<i>N</i> vs. AD1	AD1 vs. AD2	<i>N</i> vs. AD2
1	R3-C4 <sub>1</sub>	R2-F7 <sub>2</sub>	R2-F7 <sub>3</sub>	R2-Oz <sub>4</sub>	R3-C4 <sub>5</sub>
2	R3-P3 <sub>1</sub>	R3-F7 <sub>2</sub>	R1oR2-F7 <sub>3</sub>	R2-Fz <sub>4</sub>	R3-P3 <sub>5</sub>
3	R3-Fz <sub>1</sub>	R2-C4 <sub>2</sub>	R1oR3-Oz <sub>3</sub>	R2-F4 <sub>4</sub>	R3-C3 <sub>5</sub>
4	R3-Oz <sub>1</sub>	R1-C4 <sub>2</sub>	R1oR3-Pz <sub>3</sub>	R2-P3 <sub>4</sub>	R3-F3 <sub>5</sub>
5	R3-F3 <sub>1</sub>	R3-C4 <sub>2</sub>	R1oR3-O2 <sub>3</sub>	R3oR2-C3 <sub>4</sub>	R3-P4 <sub>5</sub>
6	R3-C3 <sub>1</sub>	R1-F7 <sub>2</sub>	R2-C4 <sub>3</sub>	R2-F3 <sub>4</sub>	R3-T4 <sub>5</sub>
7	R3-F4 <sub>1</sub>	R2-T4 <sub>2</sub>	R1oR3-O1 <sub>3</sub>	R4oR2-C3 <sub>4</sub>	R2-C4 <sub>5</sub>
8	R3-P4 <sub>1</sub>	R4-C4 <sub>2</sub>	R2-T3 <sub>3</sub>	R2-C3 <sub>4</sub>	R3-F4 <sub>5</sub>
9	R3-Cz <sub>1</sub>	R2-F3 <sub>2</sub>	R1oR2-T4 <sub>3</sub>	R2-O2 <sub>4</sub>	R2-F3 <sub>5</sub>
10	R3-T4 <sub>1</sub>	R2-T3 <sub>2</sub>	R1oR2-C4 <sub>3</sub>	R2-Pz <sub>4</sub>	R3-Oz <sub>5</sub>
11	R3-O1 <sub>1</sub>	R3-T4 <sub>2</sub>	R1oR2-C3 <sub>3</sub>	R5oR2-C3 <sub>4</sub>	R3-Fz <sub>5</sub>
12	R3-O2 <sub>1</sub>	R3-F3 <sub>2</sub>	R1oR2-F3 <sub>3</sub>	R2-O1 <sub>4</sub>	R2-P3 <sub>5</sub>
13	R3-Pz <sub>1</sub>	R2-T6 <sub>2</sub>	R2-T6 <sub>3</sub>	R3oR1-C3 <sub>4</sub>	R2-T4 <sub>5</sub>
14	R2-C4 <sub>1</sub>	R1-T4 <sub>2</sub>	R3-F7 <sub>3</sub>	R2-Cz <sub>4</sub>	R1-F3 <sub>5</sub>
15	R1-F7 <sub>1</sub>	R2oR3-F8 <sub>2</sub>	R1oR2-T3 <sub>3</sub>	R1oR2-C3 <sub>4</sub>	R3-T5 <sub>5</sub>
16	R2-F3 <sub>1</sub>	R3-T3 <sub>2</sub>	R2-T4 <sub>3</sub>	R1oR2-F7 <sub>4</sub>	R3-O1 <sub>5</sub>
17	R2-fz <sub>1</sub>	R4-F7 <sub>2</sub>	R1oR3-Fp1 <sub>3</sub>	R5oR3-C3 <sub>4</sub>	R1-C4 <sub>5</sub>
18	R1-C4 <sub>1</sub>	R2-C3 <sub>2</sub>	R1oR2-T6 <sub>3</sub>	R2-P4 <sub>4</sub>	R2-Fz <sub>5</sub>
19	R1-F3 <sub>1</sub>	R4-T4 <sub>2</sub>	R1oR3-P4 <sub>3</sub>	R3oR2-F7 <sub>4</sub>	R3-T6 <sub>5</sub>
20	R2-P3 <sub>1</sub>	R2oR3-F7 <sub>2</sub>	R3oR2-T3 <sub>3</sub>	R4oR1-C3 <sub>4</sub>	R2-C3 <sub>5</sub>
21	R1-T4 <sub>1</sub>	R1-F3 <sub>2</sub>	R3oR2-F7 <sub>3</sub>	R5oR4-C3 <sub>4</sub>	R3-Cz <sub>5</sub>
22	R2-T4 <sub>1</sub>	R3-T6 <sub>2</sub>	R1oR2-Fp1 <sub>3</sub>	R2-C4 <sub>4</sub>	R1-T4 <sub>5</sub>
23	R3-T5 <sub>1</sub>	R2-P3 <sub>2</sub>	R1oR2-T5 <sub>3</sub>	R1-Oz <sub>4</sub>	R2-F4 <sub>5</sub>
24	R2-F4 <sub>1</sub>	R2oR3-T4 <sub>2</sub>	R1oR2-F8 <sub>3</sub>	R5oR3-T5 <sub>4</sub>	R2-P4 <sub>5</sub>
<i>Number of features per brain region—experiment 1 settings</i>					
Frontal	8	9	8	5	7
Central	5	5	3	11	6
Temporal	4	9	8	1	5
Parietal	4	1	2	3	4
Occipital	3	0	3	4	2

frequencies, hence a finding also not previously found via visual inspection. For space limitations, we omit the features selected via the other two experiments, but they were similar to those found in Experiment 1 and 4.

**3.5. Overall Classification Accuracy.** Lastly, using the top-24 features, Table 7 shows the final accuracy and F1 scores obtained for each of the four experiments and five classification tasks. The results achieved with the benchmark, i.e., the visually obtained power modulation spectrogram patch features from reference [29], are also added for comparisons. As can be seen, the proposed features outperformed the state-of-the-art benchmark on all five tasks by a substantial margin, with the exception of the *N* vs. AD1 task where only a subtle improvement was obtained with the experiment 4 settings. Overall, these results suggest that making the mask generic (i.e., settings in experiments 1 and 4) can lead to improved accuracy on unseen data. This was the case for four out of the five tasks, with the exception being the *N* vs. AD2 task, where experiment 2 settings resulted in the best results. Ultimately, having very specialized maps (e.g., as in experiment 3 settings) did not lead to accuracy levels that could not be achieved with other less specialized settings.

**3.6. Age-Related Confounds.** Ultimately, it is important to gauge if the proposed features are indeed measuring neural changes due to AD and not solely due to normal aging. Such

evaluation is particularly important in settings where age matching is not possible between groups, as is the case herein. Previous studies have shown a direct link between normal aging and changes in EEG powers and frequencies (e.g., see [58, 59]), thus we explore a linear mapping between the proposed feature and age and test if the obtained results correspond to those obtained from a random mapping function. Table 8 shows the root mean square errors (between estimated and true age) obtained for the Experiment 1 and Experiment 4 settings. None of the tests showed significant differences from chance at a 99% confidence level, thus suggesting that the proposed features are not capturing normal aging-related changes in the EEG and are indeed capturing neurodegenerative insights. Similar findings were found for the other two experiment settings and are omitted here for the sake of brevity.

**3.7. Study Limitations and Future Work.** The results reported in this study were performed on a limited sample size of 54 participants. While the results are promising, they need to be validated on a larger dataset. Open-source EEG datasets for AD are not widely available; thus, future work should focus on creating open-source datasets. The recent international push to enable EEG as a clinical biomarker [16] may enable more widespread collection that will help push the research forward. Furthermore, as is widely known, the machine

TABLE 6: Top 24 features selected using experiment 4 settings.

Rankings	N vs. AD1 vs. AD2	N vs. AD	N vs. AD1	AD1 vs. AD2	N vs. AD2
1	R2-Oz <sub>1</sub>	R4oR3-O1 <sub>2</sub>	R1-Fp2 <sub>3</sub>	R1-Fz <sub>4</sub>	R4-C3 <sub>5</sub>
2	R2-Fz <sub>1</sub>	R4-F7 <sub>2</sub>	R1-Pz <sub>3</sub>	R1-Oz <sub>4</sub>	R4-P3 <sub>5</sub>
3	R2-P3 <sub>1</sub>	R4oR3-Pz <sub>2</sub>	R1-Fz <sub>3</sub>	R1-F4 <sub>4</sub>	R4-T5 <sub>5</sub>
4	R2-P4 <sub>1</sub>	R4oR2-C4 <sub>2</sub>	R2oR3-Oz <sub>3</sub>	R1oR4-Fz <sub>4</sub>	R4-P4 <sub>5</sub>
5	R2-C4 <sub>1</sub>	R4oR3-Oz <sub>2</sub>	R1-O2 <sub>3</sub>	R1-P3 <sub>4</sub>	R4-O1 <sub>5</sub>
6	R2-F4 <sub>1</sub>	R4oR2-T6 <sub>2</sub>	R1oR3-Pz <sub>3</sub>	R1-F3 <sub>4</sub>	R4-C4 <sub>5</sub>
7	R2-F3 <sub>1</sub>	R4-C4 <sub>2</sub>	R2oR3-O1 <sub>3</sub>	R1-O2 <sub>4</sub>	R4oR3-C3 <sub>5</sub>
8	R2-O2 <sub>1</sub>	R4oR2-T5 <sub>2</sub>	R1-Cz <sub>3</sub>	R3-Oz <sub>4</sub>	R4-F3 <sub>5</sub>
9	R2-Pz <sub>1</sub>	R4oR2-T3 <sub>2</sub>	R2oR3-O2 <sub>3</sub>	R3-Fz <sub>4</sub>	R4-Oz <sub>5</sub>
10	R2oR3-Fz <sub>1</sub>	R4-T4 <sub>2</sub>	R2oR3-P4 <sub>3</sub>	R1-Pz <sub>4</sub>	R4oR3-F3 <sub>5</sub>
11	R2oR3-F3 <sub>1</sub>	R2oR1-O1 <sub>2</sub>	R1-Oz <sub>3</sub>	R1oR4-Oz <sub>4</sub>	R4-T4 <sub>5</sub>
12	R2-C3 <sub>1</sub>	R4oR2-O1 <sub>2</sub>	R2oR3-Pz <sub>3</sub>	R1-Cz <sub>4</sub>	R4-T6 <sub>5</sub>
13	R2-O1 <sub>1</sub>	R4oR2-P4 <sub>2</sub>	R1oR3-Oz <sub>3</sub>	R1-C3 <sub>4</sub>	R4-F7 <sub>5</sub>
14	R2-Cz <sub>1</sub>	R4oR2-T4 <sub>2</sub>	R2-O2 <sub>3</sub>	R1-O1 <sub>4</sub>	R4-O2 <sub>5</sub>
15	R2oR3-C3 <sub>1</sub>	R4oR3-F4 <sub>2</sub>	R1oR3-O2 <sub>3</sub>	R1oR4-F3 <sub>4</sub>	R4-Pz <sub>5</sub>
16	R2oR3-Oz <sub>1</sub>	R2oR1-O2 <sub>2</sub>	R1oR3-Fp1 <sub>3</sub>	R1oR4-F4 <sub>4</sub>	R4-F4 <sub>5</sub>
17	R2oR3-C4 <sub>1</sub>	R5oR2-C4 <sub>2</sub>	R1oR3-Fp2 <sub>3</sub>	R1oR4-C3 <sub>4</sub>	R4oR3-T4 <sub>5</sub>
18	R2oR3-F4 <sub>1</sub>	R4oR3-O2 <sub>2</sub>	R2-T5 <sub>3</sub>	R1-P4 <sub>4</sub>	R4oR3-C4 <sub>5</sub>
19	R2oR3-P3 <sub>1</sub>	R4oR3-Fp1 <sub>2</sub>	R1oR3-Fz <sub>3</sub>	R1oR4-P3 <sub>4</sub>	R4oR3-O1 <sub>5</sub>
20	R2-T4 <sub>1</sub>	R4oR5-O1 <sub>2</sub>	R2-O1 <sub>3</sub>	R3oR4-Fz <sub>4</sub>	R4oR3-P3 <sub>5</sub>
21	R1oR3-F3 <sub>1</sub>	R4-T6 <sub>2</sub>	R2-P4 <sub>3</sub>	R1oR4-O1 <sub>4</sub>	R4-T3 <sub>5</sub>
22	R2oR3-cz <sub>1</sub>	R4oR2-P3 <sub>2</sub>	R1oR3-T3 <sub>3</sub>	R3oR2-C3 <sub>4</sub>	R4-Fz <sub>5</sub>
23	R2oR3-O1 <sub>1</sub>	R4oR3-P4 <sub>2</sub>	R1oR2-T6 <sub>3</sub>	R1-C4 <sub>4</sub>	R4oR3-F4 <sub>5</sub>
24	R1-C4 <sub>1</sub>	R4-P3 <sub>2</sub>	R2-Oz <sub>3</sub>	R1oR4-Pz <sub>4</sub>	R4-Cz <sub>5</sub>
<i>Number of features per brain region—experiment 4 settings</i>					
Frontal	7	3	5	8	6
Central	7	3	1	5	5
Temporal	1	6	3	0	5
Parietal	4	5	5	5	4
Occipital	5	7	10	6	4

TABLE 7: Performance comparison achieved with best threshold-cluster settings and top-24 features. Bold values indicate the highest accuracy achieved for a given classification task.

Tasks	Benchmark [29]		Proposed (exp. 1)		Proposed (exp. 2)		Proposed (exp. 3)		Proposed (exp. 4)	
	Acc (%)	F1 (%)	Acc (%)	F1 (%)	Acc (%)	F1 (%)	Acc (%)	F1 (%)	Acc (%)	F1 (%)
T1	50 ± 3	50 ± 3	<b>54 ± 2</b>	<b>55 ± 2</b>	<b>54 ± 2</b>	<b>55 ± 2</b>	<b>54 ± 2</b>	<b>55 ± 2</b>	47 ± 2	49 ± 2
T2	70 ± 1	65 ± 1	60 ± 2	49 ± 3	60 ± 2	49 ± 3	<b>71 ± 2</b>	<b>61 ± 2</b>	<b>71 ± 2</b>	<b>61 ± 2</b>
T3	64 ± 3	63 ± 3	48 ± 2	48 ± 2	46 ± 2	46 ± 2	46 ± 4	46 ± 4	<b>65 ± 2</b>	<b>64 ± 2</b>
T4	73 ± 2	71 ± 2	<b>83 ± 2</b>	<b>83 ± 2</b>	82 ± 0	82 ± 0	<b>83 ± 1</b>	<b>83 ± 1</b>	79 ± 1	79 ± 1
T5	73 ± 2	72 ± 2	86 ± 3	86 ± 3	<b>89 ± 3</b>	<b>89 ± 3</b>	85 ± 3	84 ± 3	82 ± 2	81 ± 2

Bold values indicate the highest accuracy achieved for a given classification task.

TABLE 8: Age prediction accuracy comparison against a random regression model for experiment 1 and experiment 4 settings.

Tasks	Exp. 1		Exp. 4	
	Nonrandom	Random	Nonrandom	Random
T1	10.33 ± 2.02	9.94 ± 1.55	9.82 ± 1.65	9.71 ± 1.75
T2	9.83 ± 1.85	9.74 ± 1.45	9.40 ± 1.69	9.48 ± 1.65
T3	8.05 ± 1.20	8.55 ± 1.55	7.81 ± 1.18	8.19 ± 1.36
T4	9.74 ± 2.77	9.30 ± 2.42	9.70 ± 2.64	9.26 ± 2.63
T5	12.19 ± 2.63	11.97 ± 2.14	11.28 ± 1.82	11.63 ± 2.46

learning algorithms are sensitive to hyper-parameter tuning. Since the data available for this study was limited, not much effort was spent on parameter optimization; hence, the accuracy results reported may not be the highest achievable with the proposed feature set. Once more data become

available, future work could explore the overall impact of hyperparameter tuning on classification accuracy. Moreover, in this study, saliency maps per channel were obtained, but an average map was used for simplified feature importance selection. Once more data becomes available, per-

channel optimized feature patches may be used, resulting in improved accuracy. It is known that degeneration due to AD can spread to different brain regions as the disease progresses, hence it is expected that different regional saliency maps will be useful for the different tasks explored herein. This channel-aware optimization may also lead to an overall system that can rely on a subset of the EEG channels, hence, enabling the creation of a portable, low-density, and low-cost solution, as in [69], that could help tackle AD worldwide.

Moreover, here we explored AD1 vs. AD2 discrimination, hence, obtaining insights on how disease severity can change the EEG patterns used in biomarker development. Ultimately, future work should explore neural changes seen in longitudinal studies where data from one patient's progression is monitored, thus truly leading to disease progression insights. For example, it is known that roughly a quarter of patients with mild cognitive impairment (MCI) will progress to AD within a 4-year window. Understanding the neural signature changes between MCI patients that do progress to AD and those that do not could provide useful clues not only for disease progression but also for the risk associated with developing AD at very early stages. Lastly, recent studies have shown that EEG combined with MRI could lead to useful insights for disease severity level prediction [70]. On that study, the authors showed the complementarity of the visually obtained patch features with anatomical features extracted from MRIs to predict the MMSE scores of the patients. Future work should explore the benefits of combining the proposed features with MRI ones to quantify the gains that can be achieved.

#### 4. Conclusions

In this article, we have proposed the use of a convolutional neural network (CNN) combined with saliency maps, trained on an image-like power modulation spectrogram of eyes-closed resting-state EEGs, to find new biomarkers of Alzheimer's disease. The goal was to explore if a data-driven biomarker selection method could provide insights complementary to those obtained via visual inspection. In particular, we explored biomarkers for five classification tasks: healthy ( $N$ ) vs. mild-AD (AD1) vs. moderate-to-severe AD (AD2), (2)  $N$  vs. AD (combined AD1 and AD2), (3)  $N$  vs. AD1, (4) AD1 vs. AD2, and (5)  $N$  vs. AD2. The biomarkers found were extracted for each of the available EEG channels and reduced to the top 24 features via feature selection before being input to a support vector machine for final classification. The most important brain regions found coincided with those widely reported in the AD literature, and most importantly, the power modulation spectrogram patches complemented those found previously via visual inspection. Overall, the proposed method outperformed the benchmark on all five classification tasks and by a large margin. To assure the newly-proposed features were not measuring EEG changes due to normal aging, results were compared to a random age prediction classifier and no significant differences were found.

#### Data Availability

The data used to support the findings of this study are available upon request to Tiago.Falk@inrs.ca.

#### Disclosure

The work presented in this study has been conducted and presented by the first author during her master thesis research [71]. The thesis has already been defended and shows up publicly at the institution's website. However, the authors would like to declare that this work is original and has not been published or submitted to any other journals.

#### Conflicts of Interest

The authors declare that they have no conflicts of interest.

#### Acknowledgments

The authors would like to thank Prof. F. Fraga (UFABC) and Dr. R. Anghinah (USP) for making the EEG database available and for earlier collaborations on EEG signal processing. The authors also acknowledge funding from NSERC Canada under the Discovery Grants program (RGPIN-2016-04175).

#### References

- [1] R. S. Wilson, E. Segawa, P. A. Boyle, S. E. Anagnos, L. P. Hizel, and D. A. Bennett, "The natural history of cognitive decline in Alzheimer's disease," *Psychology and Aging*, vol. 27, no. 4, pp. 1008–1017, 2012.
- [2] W. W. Barker, C. A. Luis, A. Kashuba et al., "Relative frequencies of Alzheimer disease, lewy body, vascular and frontotemporal dementia, and hippocampal sclerosis in the State of Florida Brain Bank," *Alzheimer Disease and Associated Disorders*, vol. 16, no. 4, pp. 203–212, 2002.
- [3] R. A. Sperling, P. S. Aisen, L. A. Beckett et al., "Toward defining the preclinical stages of Alzheimer's disease: recommendations from the National Institute on Aging-Alzheimer's Association workgroups on diagnostic guidelines for Alzheimer's disease," *Alzheimer's and Dementia*, vol. 7, no. 3, pp. 280–292, 2011.
- [4] R. Sperling, E. Mormino, and K. Johnson, "The evolution of preclinical Alzheimer's disease: implications for prevention trials," *Neuron*, vol. 84, no. 3, pp. 608–622, 2014.
- [5] M. Prince, R. Bryce, and C. Ferri, *World Alzheimer Report 2011: The Benefits of Early Diagnosis and Intervention*, Alzheimer's Disease International, London, 2018.
- [6] H. Rania M, E. Ammar, I. Mohamed et al., "Alzheimer's disease and its current treatments; Is there a possibility for a cure?" *Open Journal of Chemistry*, vol. 5, no. 1, pp. 013–019, 2019.
- [7] A. Singh, P. Deshpande, and N. Gogia, "Exploring the efficacy of natural products in alleviating Alzheimer's disease," *Neural regeneration research*, vol. 14, no. 8, p. 1321, 2019.
- [8] K. G. Yiannopoulou and S. G. Papageorgiou, "Current and future treatments in Alzheimer disease: an update," *Journal of Central Nervous System Disease*, vol. 12, Article ID 117957352090739, 2020.
- [9] A. J. Mitchell, "A meta-analysis of the accuracy of the mini-mental state examination in the detection of dementia and








- mild cognitive impairment,” *Journal of Psychiatric Research*, vol. 43, no. 4, pp. 411–431, 2009.
- [10] J. C. Morris, “Current vision and scoring rules the clinical dementia rating (CDR),” *Neurology*, vol. 43, pp. 2412–2414, 1993.
- [11] G. Chetelat and J.-C. Baron, “Early diagnosis of Alzheimer’s disease: contribution of structural neuroimaging,” *Neuro-Image*, vol. 18, no. 2, pp. 525–541, 2003.
- [12] G. B. Frisoni, N. C. Fox, C. R. Jack, P. Scheltens, and P. M. Thompson, “The clinical use of structural mri in Alzheimer disease,” *Nature Reviews Neurology*, vol. 6, no. 2, pp. 67–77, 2010.
- [13] R. Mayeux and N. Schupf, “Blood-based biomarkers for Alzheimer’s disease: plasma A $\beta$ 40 and A $\beta$ 42, and genetic variants $\beta$ 40 and a  $\beta$ 42, and genetic variants,” *Neurobiology of Aging*, vol. 32, pp. S10–S19, 2011.
- [14] A. Caroli and G. Frisoni, “The dynamics of Alzheimer’s disease biomarkers in the Alzheimer’s Disease Neuroimaging Initiative cohort,” *Neurobiology of Aging*, vol. 31, no. 8, pp. 1263–1274, 2010.
- [15] C. Van Cauwenbergh, C. Van Broeckhoven, and K. Sleegers, “The genetic landscape of Alzheimer disease: clinical implications and perspectives,” *Genetics in Medicine*, vol. 18, no. 5, pp. 421–430, 2016.
- [16] P. M. Rossini, R. Di Iorio, F. Vecchio et al., “Early diagnosis of Alzheimer’s disease: the role of biomarkers including advanced EEG signal analysis. report from the IFCN-sponsored panel of experts,” *Clinical Neurophysiology*, vol. 131, no. 6, pp. 1287–1310, 2020.
- [17] F. Maestú, P. Cuesta, O. Hasan, A. Fernández, M. Funke, and P. E. Schulz, “The importance of the validation of M/EEG with current biomarkers in Alzheimer’s disease,” *Frontiers in Human Neuroscience*, vol. 13, p. 17, 2019.
- [18] F. Vecchio, C. Babiloni, R. Lizio et al., “Resting state cortical EEG rhythms in Alzheimer’s disease: toward EEG markers for clinical applications: a review,” *Supplements to Clinical Neurophysiology*, vol. 62, pp. 223–236, 2013.
- [19] R. Cassani, M. Estarellas, R. San-Martin, F. J. Fraga, and T. H. Falk, “Systematic review on resting-state EEG for Alzheimer’s disease diagnosis and progression assessment,” *Disease Markers*, vol. 2018, Article ID 5174815, 2018.
- [20] M. Alessandrini, G. Biagetti, P. Crippa, L. Falaschetti, S. Luzzi, and C. Turchetti, “Eeg-based alzheimer’s disease recognition using robust-pca and lstm recurrent neural network,” *Sensors*, vol. 22, no. 10, p. 3696, 2022.
- [21] K. AlSharabi, Y. Bin Salamah, A. M. Abdurraqeab, M. Aljalal, and F. A. Alturki, “Eeg signal processing for alzheimer’s disorders using discrete wavelet transform and machine learning approaches,” *IEEE Access*, vol. 10, Article ID 89781, 89797 pages, 2022.
- [22] D. Pirrone, E. Weitschek, P. Di Paolo, S. De Salvo, and M. C. De Cola, “Eeg signal processing and supervised machine learning to early diagnose alzheimer’s disease,” *Applied Sciences*, vol. 12, no. 11, p. 5413, 2022.
- [23] T. H. Falk, F. J. Fraga, L. Trambaiolli, and R. Anghinah, “EEG amplitude modulation analysis for semi-automated diagnosis of Alzheimer’s disease,” *EURASIP Journal on Applied Signal Processing*, vol. 2012, no. 1, Article ID 192, 199 pages, 2012.
- [24] F. J. Fraga, T. H. Falk, P. A. M. Kanda, and R. Anghinah, “Characterizing Alzheimer’s disease severity via resting-awake EEG amplitude modulation analysis,” *PLoS One*, vol. 8, no. 8, Article ID e72240, 2013.
- [25] R. Cassani, T. H. Falk, F. J. Fraga, P. A. M. Kanda, and R. Anghinah, “The effects of automated artifact removal algorithms on electroencephalography-based Alzheimer’s disease diagnosis,” *Frontiers in Aging Neuroscience*, vol. 6, p. 55, 2014.
- [26] P. L. Nunez, R. Srinivasan, and D. Chen, *Electric fields of the Brain: The Neurophysics of EEG*, Oxford University Press, USA, 2006.
- [27] M. Elgendi, F. Vialatte, A. Cichocki, C. Latchoumane, J. Jeong, and J. Dauwels, “Optimization of EEG frequency bands for improved diagnosis of Alzheimer disease,” in *Proceedings of the 2011 Annual International Conference of the IEEE Engineering in Medicine and Biology Society*, pp. 6087–6091, IEEE, Boston, MA, USA, August 2011.
- [28] E. Gallego-Jutglà, J. Solé-Casals, F.-B. Vialatte, M. Elgendi, A. Cichocki, and J. Dauwels, “A hybrid feature selection approach for the early diagnosis of Alzheimer’s disease,” *Journal of Neural Engineering*, vol. 12, no. 1, Article ID 016018, 2015.
- [29] R. Cassani and T. H. Falk, “Alzheimer’s disease diagnosis and severity level detection based on electroencephalography modulation spectral “patch” features,” *IEEE journal of biomedical and health informatics*, vol. 24, no. 7, pp. 1982–1993, 2020.
- [30] K. Simonyan, A. Vedaldi, and A. Zisserman, “Deep inside Convolutional Networks: Visualising Image Classification Models and Saliency Maps,” 2013, <https://arxiv.org/abs/1312.6034>.
- [31] A. Pulido, A. Rueda, and E. Romero, “Classification of Alzheimer’s disease using regional saliency maps from brain MR volumes,” *Medical Imaging 2013: Computer-Aided Diagnosis*, vol. 8670, Article ID 86700R, 2013.
- [32] O. Ben-Ahmed, F. Lecellier, M. Paccalin, and C. Fernandez-Maloigne, “Multi-view visual saliency-based MRI classification for Alzheimer’s disease diagnosis,” in *Proceedings of the 2017 Seventh International Conference on Image Processing Theory, Tools and Applications (IPTA)*, pp. 1–6, IEEE, Montreal, QC, Canada, November 2017.
- [33] G. Mckhann, D. Drachman, M. Folstein, R. Katzman, D. Price, and E. M. Stadlan, “Clinical diagnosis of alzheimer’s disease: report of the NINCDS-ADRDA work group\* under the auspices of department of health and human services task force on alzheimer’s disease,” *Neurology*, vol. 34, no. 7, pp. 939–944, 1984.
- [34] S. M. Brucki, R. Nitrini, P. Caramelli, P. H. Bertolucci, and I. H. Okamoto, “Sugestões para o uso do mini-exame do estado mental no Brasil,” *Arquivos de neuro-psiquiatria*, vol. 61, no. 3B, pp. 777–781, 2003.
- [35] N. P. Castellanos and V. A. Makarov, “Recovering EEG brain signals: artifact suppression with wavelet enhanced independent component analysis,” *Journal of Neuroscience Methods*, vol. 158, no. 2, pp. 300–312, 2006.
- [36] M. T. Akhtar, W. Mitsuhashi, and C. J. James, “Employing spatially constrained ICA and wavelet denoising, for automatic removal of artifacts from multichannel EEG data,” *Signal Processing*, vol. 92, no. 2, pp. 401–416, 2012.
- [37] L. R. Trambaiolli, T. H. Falk, F. J. Fraga, R. Anghinah, and A. C. Lorena, “EEG spectro-temporal modulation energy: a new feature for automated diagnosis of Alzheimer’s disease,” in *Proceedings of the 2011 Annual International Conference of the IEEE Engineering in Medicine and Biology Society*, pp. 3828–3831, IEEE, Boston, MA, USA, August 2011.
- [38] L. Atlas and S. A. Shamma, “Joint acoustic and modulation frequency,” *EURASIP Journal on Applied Signal Processing*, vol. 2003, no. 7, Article ID 310290, 310298 pages, 2003.

- [39] R. Cassani and T. H. Falk, *Spectrotemporal Modeling of Biomedical Signals: Theoretical Foundation and Applications, Reference Module In Biomedical Sciences*, Elsevier, Amsterdam, The Netherlands, 2018.
- [40] J. Patterson and A. Gibson, *Deep Learning: A Practitioner's Approach*, O'Reilly Media, Inc, Sebastopol, California, 2017.
- [41] Y. LeCun, K. Kavukcuoglu, and C. Farabet, "Convolutional networks and applications in vision," in *Proceedings of the 2010 IEEE International Symposium on Circuits and Systems*, pp. 253–256, IEEE, Paris, France, May 2010.
- [42] K. O'Shea and R. Nash, "An Introduction to Convolutional Neural Networks," 2015, <https://arxiv.org/abs/1511.08458>.
- [43] J. Koushik, "Understanding Convolutional Neural Networks," 2016, <https://arxiv.org/abs/1605.09081>.
- [44] S. J. Plathottam, H. Salehfar, and P. Ranganathan, "Convolutional Neural Networks (CNNs) for power system big data analysis," in *Proceedings of the 2017 North American Power Symposium (NAPS)*, pp. 1–6, IEEE, Morgantown, WV, USA, September 2017.
- [45] I. Goodfellow, Y. Bengio, and A. Courville, *Deep Learning*, MIT press, Cambridge, Massachusetts, 2016.
- [46] G. Litjens, T. Kooi, B. E. Bejnordi et al., "A survey on deep learning in medical image analysis," *Medical Image Analysis*, vol. 42, pp. 60–88, 2017.
- [47] L. Brocki and N. C. Chung, "Concept saliency maps to visualize relevant features in deep generative models," in *Proceedings of the 2019 18th IEEE International Conference on Machine Learning and Applications (ICMLA)*, pp. 1771–1778, IEEE, Boca Raton, FL, USA, December 2019.
- [48] S. Banerjee, S. Mitra, B. U. Shankar, and Y. Hayashi, "A novel GBM saliency detection model using multi-channel MRI," *PLoS One*, vol. 11, no. 1, Article ID e0146388, 2016.
- [49] S. Mitra, S. Banerjee, and Y. Hayashi, "Volumetric brain tumour detection from MRI using visual saliency," *PLoS One*, vol. 12, no. 11, Article ID e0187209, 2017.
- [50] B. Rasolzadeh, M. Björkman, K. Huebner, and D. Kragic, "An active vision system for detecting, fixating and manipulating objects in the real world," *The International Journal of Robotics Research*, vol. 29, no. 2-3, pp. 133–154, 2010.
- [51] S. Ramenahalli, "A biologically motivated, proto-object-based audiovisual saliency model," *A&I*, vol. 1, no. 4, pp. 487–509, 2020.
- [52] S. Ramenahalli, D. R. Mendat, S. Dura-Bernal, E. Culurciello, E. Niebur, and A. Andreou, "Audio-visual saliency map: overview, basic models and hardware implementation," in *Proceedings of the 2013 47th Annual Conference on Information Sciences and Systems (CISS)*, pp. 1–6, IEEE, Baltimore, MD, USA, March 2013.
- [53] R. Henderson and R. Rothe, "Picasso: A Modular Framework for Visualizing the Learning Process of Neural Network Image Classifiers," 2017, <https://arxiv.org/abs/1705.05627>.
- [54] R. Cassani and T. H. Falk, "Automated alzheimer's disease diagnosis using a low-density EEG layout and new features based on the power of modulation spectral "patches"," in *Proceedings of the 2019 IEEE International Conference on Systems, Man and Cybernetics (SMC)*, pp. 1259–1263, IEEE, Bari, Italy, October 2019.
- [55] A. J. Smola and B. Schölkopf, "A tutorial on support vector regression," *Statistics and Computing*, vol. 14, no. 3, pp. 199–222, 2004.
- [56] R. Guerreiro and J. Bras, "The age factor in Alzheimer's disease," *Genome Medicine*, vol. 7, no. 1, 2015.
- [57] C. Sala Frigerio, L. Wolfs, N. Fattorelli et al., "The major risk factors for alzheimer's disease: age, sex, and genes modulate the microglia response to a  $\beta$  plaques $\beta$ plaques," *Cell Reports*, vol. 27, no. 4, pp. 1293–1306.e6, 2019.
- [58] J. Polich, "EEG and ERP assessment of normal aging," *Electroencephalography and Clinical Neurophysiology: Evoked Potentials Section*, vol. 104, no. 3, pp. 244–256, 1997.
- [59] J. Polich, "On the relationship between EEG and P300: individual differences, aging, and ultradian rhythms," *International Journal of Psychophysiology*, vol. 26, no. 1-3, pp. 299–317, 1997.
- [60] S. T. DeKosky and S. W. Scheff, "Synapse loss in frontal cortex biopsies in Alzheimer's disease: correlation with cognitive severity," *Annals of Neurology*, vol. 27, no. 5, pp. 457–464, 1990.
- [61] B. C. Dickerson, A. Bakkour, D. H. Salat et al., "The cortical signature of Alzheimer's disease: regionally specific cortical thinning relates to symptom severity in very mild to mild ad dementia and is detectable in asymptomatic amyloid-positive individuals," *Cerebral Cortex*, vol. 19, no. 3, pp. 497–510, 2009.
- [62] S. Rathore, M. Habes, M. A. Iftikhar, A. Shacklett, and C. Davatzikos, "A review on neuroimaging-based classification studies and associated feature extraction methods for Alzheimer's disease and its prodromal stages," *NeuroImage*, vol. 155, pp. 530–548, 2017.
- [63] M. G. Knyazeva, M. Jalili, A. Brioschi et al., "Topography of EEG multivariate phase synchronization in early Alzheimer's disease," *Neurobiology of Aging*, vol. 31, no. 7, pp. 1132–1144, 2010.
- [64] J. A. van Deursen, E. F. P. M. Vuurman, F. R. J. Verhey, V. H. J. M. van Kranen-Mastenbroek, and W. J. Riedel, "Increased EEG gamma band activity in Alzheimer's disease and mild cognitive impairment," *Journal of Neural Transmission*, vol. 115, no. 9, pp. 1301–1311, 2008.
- [65] L. R. Trambaiolli, R. Cassani, and T. H. Falk, "Eeg spectrotemporal amplitude modulation as a measurement of cortical hemodynamics: an eeg-fnirs study," in *Proceedings of the 2020 42nd Annual International Conference of the IEEE Engineering in Medicine and Biology Society (EMBC)*, pp. 3481–3484, IEEE, Montreal, QC, Canada, July 2020.
- [66] K. Kisler, A. R. Nelson, A. Montagne, and B. V. Zlokovic, "Cerebral blood flow regulation and neurovascular dysfunction in alzheimer disease," *Nature Reviews Neuroscience*, vol. 18, no. 7, pp. 419–434, 2017.
- [67] J. C. de la Torre, "Cerebral hemodynamics and vascular risk factors: setting the stage for alzheimer's disease," *Journal of Alzheimer's Disease*, vol. 32, no. 3, pp. 553–567, 2012.
- [68] M. Penttilä, J. V. Partanen, H. Soininen, and P. Riekinen, "Quantitative analysis of occipital EEG in different stages of Alzheimer's disease," *Electroencephalography and Clinical Neurophysiology*, vol. 60, no. 1, pp. 1–6, 1985.
- [69] R. Cassani, T. H. Falk, F. J. Fraga, M. Cecchi, D. K. Moore, and R. Anghinah, "Towards automated electroencephalography-based Alzheimer's disease diagnosis using portable low-density devices," *Biomedical Signal Processing and Control*, vol. 33, pp. 261–271, 2017.
- [70] B. De Jesus Junior, R. Cassani, W. J. McGeown, M. Cecchi, K. Fadem, and T. H. Falk, "Multimodal prediction of alzheimer's disease severity level based on resting-state EEG and structural MRI," *Frontiers in Human Neuroscience*, vol. 495, 2020.
- [71] M. K. Soares Lopes, "On the use of saliency maps for improved modulation spectral patch features for alzheimer's disease diagnosis," Ph.D. dissertation, Maîtrise en télécommunications, New York City, 2021.



## Research Article

# Increased Risk of Suicide among Cancer Survivors Who Developed a Second Malignant Neoplasm

Huazhen Yang <sup>1,2</sup>, Yuanyuan Qu <sup>1,2</sup>, Yanan Shang <sup>1,2</sup>, Chengshi Wang <sup>3,4</sup>,  
Junren Wang <sup>1,2</sup>, Donghao Lu <sup>1,5,6</sup>, and Huan Song <sup>1,2,7</sup>

<sup>1</sup>West China Biomedical Big Data Center, West China Hospital, Sichuan University, Chengdu, China

<sup>2</sup>Med-X Center for Informatics, Sichuan University, Chengdu, China

<sup>3</sup>Sichuan Cancer Hospital & Institute, Sichuan Cancer Center, School of Medicine, University of Electronic Science and Technology of China, Chengdu, China

<sup>4</sup>Laboratory of Molecular Diagnosis of Cancer, Clinical Research Center for Breast, West China Hospital, Sichuan University, Chengdu, China

<sup>5</sup>Institute of Environmental Medicine, Karolinska Institute, Stockholm, Sweden

<sup>6</sup>Department of Epidemiology, Harvard T. H. Chan School of Public Health, Boston, MA, USA

<sup>7</sup>Center of Public Health Sciences, Faculty of Medicine, University of Iceland, Reykjavík, Iceland

Correspondence should be addressed to Donghao Lu; [donghao.lu@ki.se](mailto:donghao.lu@ki.se) and Huan Song; [songhuan@wchscu.cn](mailto:songhuan@wchscu.cn)

Received 4 November 2021; Accepted 7 December 2021; Published 10 January 2022

Academic Editor: Guangming Zhang

Copyright © 2022 Huazhen Yang et al. This is an open access article distributed under the Creative Commons Attribution License, which permits unrestricted use, distribution, and reproduction in any medium, provided the original work is properly cited.

**Background.** Cancer diagnosis entails substantial psychological distress and is associated with dramatically increased risks of suicidal behaviors. However, little is known about the suicide risk among cancer survivors who developed a second malignant neoplasm (SMN). **Methods.** Using the Surveillance, Epidemiology, and End Results database, we conducted a population-based cohort study involving 7,824,709 patients with first malignant neoplasm (FMN). We measured the hazard ratios (HRs) of suicide death after receiving a SMN diagnosis using Cox proportional hazard models, as compared with patients with FMN. The comparison with the US population was achieved by calculating standardized mortality ratios (SMRs). **Results.** Totally 685,727 FMN patients received a diagnosis of SMN during follow-up, and we in total identified 10,930 and 937 suicide deaths among FMN and SMN patients, respectively. The HR of suicide deaths was 1.23 (95% confidence interval (CI), 1.14–1.31) after a SMN diagnosis, compared with FMN patients, after adjusting for sociodemographic factors, tumor characteristics, and cancer treatment. As compared with the general population, while both SMN and FMN patients suffered an increased risk of suicide deaths, the excess risk was higher among SMN patients than FMN patients (age-, sex-, and calendar-year-adjusted SMR 1.65 (95% CI 1.54–1.75) vs. 1.29 (95% CI 1.26–1.31);  $P_{\text{difference}} < 0.0001$ ). Notably, across different time periods, we observed the greatest risk elevation during the first 3 months after a cancer diagnosis. **Conclusions.** Compared with either patients with FMN or the general population, cancer survivors who received a SMN diagnosis were at increased risk of suicide death. The risk elevation was most prominent soon after the cancer diagnosis, highlighting the necessity of providing timely psychological support to cancer survivors with a SMN.

## 1. Introduction

A growing number of patients are surviving from cancer because of the increased survival as well as the advances in cancer screening programs and novel treatments [1–3]. However, all cancer survivors are at risk for developing a second primary cancer [4–6]. It was reported that the

incidence of second malignant neoplasm (SMN), calculated from the Surveillance, Epidemiology, and End Results (SEER) Program, was approximately 8.1% between 1992 and 2008 in the United States, indicating that nearly 1 in 12 cancer patients can develop a SMN [6].

Cancer is a devastating illness that comes with tremendous psychological distress [7–9]. Accumulating evidence has

shown that people diagnosed with cancer are at an elevated risk of suicidal behaviors, including complete suicide [10–12] and suicide attempts [13, 14], compared with the general population. Therefore, it is plausible that receiving a diagnosis of SMN, acting as a repeat and possibly stronger stressor, might further increase the risk of suicide among cancer survivors. Indeed, patients with subsequent primary cancers (i.e., two or more primary cancers) have been reported to be at elevated risk for poorer physical and mental health status (e.g., serious psychological distress) [15–18]. However, the risk of suicide among patients with SMN is unclear.

Therefore, leveraging the population-based cancer cohort from the SEER database, which has stringent criteria for identifying multiple primary neoplasms, together with the aggregated US population data and US mortality data, we aimed to examine the risk of suicide among cancer survivors who developed a SMN.

## 2. Materials and Methods

**2.1. Study Population.** The SEER Program has collected cancer incidence and survival data from population-based cancer registries since 1973, covering approximately 34% of the US population as of 2016 [19]. Information on patient demographics, year and month of diagnosis, tumor characteristics (including primary tumor site, cancer behavior, tumor size, and tumor grade), treatment utilization, and active follow-up for vital status were routinely documented [20].

In the present study, we conducted a population-based cohort study using the SEER registry records between January 1, 1975, and December 31, 2016, in the United States. Among the 9,157,072 cancer patients (Figure 1), we excluded 114,866 who were diagnosed only through autopsy or death certificate, 1,409 with no information on birth year, 1,184,919 that recorded as not their first malignancy (670,225 with no information on primary malignancy and 514,694 with no information on FMN), and 31,169 with their cancer diagnosis before age 5, leaving 7,824,709 eligible FMN patients for further analysis.

All patients were followed from the diagnosis of FMN until death, the occurrence of a subsequent malignancy, or December 31, 2016, whichever occurred first. Because the SEER data provided only survival in months for survival analysis, we assigned an average survival time of 15 days for individuals who died in the same month of diagnosis. By linking to the subsequent malignancy diagnoses in SEER, we identified 685,727 patients who developed a SMN during the follow-up who therefore were included in the exposed group. Namely, patients without a SMN diagnosis contributed all person-time to the unexposed group, while the ones with a SMN diagnosis contributed their person-time before the SMN diagnosis to the unexposed group and to the exposed group from the time of diagnosis onward.

**2.2. Ascertainment of FMN and SMN.** We first identified patients with a FMN diagnosis according to the SEER collected tumor information on the primary tumor (yes or

no), tumor behavior (malignant or not), and first malignant primary indicator (yes or no). Through linkage to the information on subsequent cancer diagnoses, we then further identified individuals with a SMN diagnosis among these FMN survivors. In a subanalysis, we performed separate analyses on prostate cancer, breast cancer, colorectal cancer, lung cancer, nonmelanoma skin cancer, cancer of the central nervous system, severe cancer (esophageal, liver, or pancreatic cancer), and other cancers, as well as lifestyle-related cancers (alcohol- and smoking-related cancers) [21], according to the International Classification of Disease Oncology (ICD-O) third edition codes (Supplementary Table 1).

**2.3. Ascertainment of Suicide.** Based on the cause-specific death classification both for SEER and US mortality data, which was derived from the death certificate, we considered individuals to have committed suicide if the cause of death was coded as suicide and self-inflicted injury, with the corresponding International Classification of Diseases (ICD) 10th edition (ICD-10) codes as U03, X60–X84, and Y87.0.

**2.4. Covariates.** Data on potential confounders, including birth year, sex, calendar year at diagnosis, sociodemographic factors (i.e., race, cohabitation status, insurance, and state), tumor characteristic (i.e., tumor size and grade), and cancer treatment (i.e., chemotherapy, radiotherapy, and surgery), were obtained from the SEER database. All missing values of the covariates were coded to the “unknown” category. The corresponding information on age at death, sex, and calendar year for the US population data were derived from the US Census Bureau’s Population Estimates Program.

**2.5. Statistical Analysis.** We assessed the relative risk of suicide in relation to SMN diagnosis compared with FMN patients, using hazard ratios (HRs) with 95% confidence intervals (CI) derived from Cox regression models. Models were partly (models 1–3) or fully (model 4) adjusted for the birth year (as a continuous variable), sex (male or female), calendar year at diagnosis (1975–1984, 1985–1994, 1995–2004, or 2005–2016), race (white, black, or others/unknown), cohabitation status (cohabitation, non-cohabitation, or unknown), insurance (insured, uninsured, or unknown), state (Alaska, California, Connecticut, Georgia, Hawaii, Iowa, Kentucky, Louisiana, Michigan, New Jersey, New Mexico, Utah, or Washington), tumor size (<1.5, ≥1.5 cm, or unknown), tumor grade (well, moderately, poorly differentiated/undifferentiated, or unknown), chemotherapy/radiotherapy (yes or no/unknown), and surgery (yes or no/unknown). We also examined the association between SMN diagnosis and subsequent risk of suicide death by cancer subtypes, after controlling for available confounders. Lifestyle factors (i.e., alcohol drinking and smoking) might modify the studied association. We therefore also separately analyzed alcohol-related cancers and smoking-related cancers.

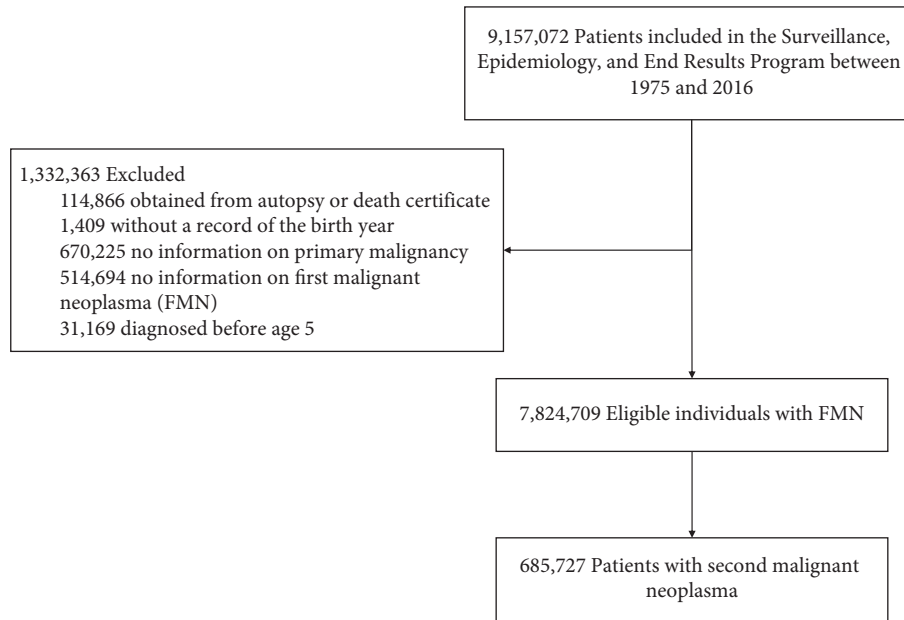


FIGURE 1: Study design.

In subgroup analyses, HRs were calculated separately by age at diagnosis (by quantile: <55, 55–65, 66–75, or >75 years), calendar year at diagnosis, sex, race, cohabitation status, tumor size, tumor grade, chemotherapy/radiotherapy, surgery, and the time interval between FMN and SMN. Furthermore, we explored whether the relative risk of suicide after a SMN diagnosis varied across different time periods since cancer diagnosis, by analyzing the associations in different follow-up periods (<1, 1–2, 3–4, 5–10, or >10 years). Additionally, we calculated the HRs by characteristics of their first malignancies (i.e., tumor characteristics and treatment utilization) to explore the potential modified role of first malignancy among SMN patients. The statistical significance of the difference between HRs was assessed by including an interaction term in the Cox model.

To better interpret our findings, we also calculated standardized mortality ratios (SMRs; i.e., the ratio of the observed to the expected number of suicide deaths) with 95% CIs to estimate the relative risk for suicide after SMN, as well as FMN, using the general US population as reference. Specifically, the number of expected suicide deaths was calculated by multiplying the observed number of person-years by age- (5 year strata), sex-, and calendar-year-specific suicide rates derived from the general US population. We further estimated SMRs by different follow-up periods (i.e.,  $\leq 1$ , 2–3, 4–6, or 7–12 months or 1–2, 3–5, 6–10, or >10 years) after the SMN or FMN diagnosis to examine the immediate and long-term impact. The statistical significance of the difference between SMRs was assessed by the heterogeneity test.

To test the robustness of the observed associations, we repeated the main analysis excluding SMN patients with a prior history of FMN at the same tumor site. We further assessed the potential influence of unmeasured confounders using the *E*-value [22]. All the analyses were conducted in R software (version 4.0). A two-sided *P*-value <0.05 was considered statistically significant.

### 3. Results

Of the 9,157,072 cancer patients in the SEER data, we identified 7,824,709 FMN patients in the population-based cohort, among which 685,727 individuals were exposed to a SMN diagnosis during up to 42 years of the follow-up period (Figure 1). With a total of 46,507,112 accumulated person-years, the median follow-up time was 1.67 (Q1–Q3: 0.42–5.00) and 3.17 (0.67–8.67) years for the SMN and FMN patients, respectively (Table 1). There was little difference in race, cohabitation status, state, and tumor grade between the SMN and FMN patients. However, compared with the FMN patients, patients with a SMN diagnosis were more likely to be male (58.97% vs. 51.28%), older (mean age 71.00 vs. 63.60 years), insured (49.46% vs. 38.82%), with larger tumor size (46.92% vs. 42.31%), and not treated (37.35% vs. 44.32% and 53.46% vs. 58.59% for chemotherapy/radiotherapy and surgery, respectively).

During follow-up, a total of 937 suicide deaths (crude incidence rate, 3.90 per 10,000 person-years) and 10,930 suicide deaths (2.48 per 10,000 person-years) were identified among SMN patients and FMN patients, respectively (Table 2). Correspondingly, we observed a consistently elevated relative risk of suicide among SMN patients compared with FMN patients across different models; the fully adjusted HR (model 4) was 1.23 (95% CI 1.14–1.31). Similar risk elevations were observed for alcohol-related cancers (HR 1.37; 95% CI 1.10–1.72; Figure 2) and smoking-related cancers (HR 1.18; 95% CI 1.06–1.31). Furthermore, among all studied cancer subtypes defined by the sites of SMN, the HRs were most pronounced when SMN was severe cancer (HR 1.97; 95% CI 1.48–2.63) or lung cancer (HR 1.57; 95% CI 1.34–1.86; Figure 2).

In a subanalysis, the excess risk of suicide in SMN patients did not differ by calendar year, sex, race, cohabitation status, tumor grade, tumor size, chemotherapy/

TABLE 1: Characteristics of the study cohort.

	SMN <sup>a</sup> (N = 685727)	FMN <sup>b</sup> (N = 7824709)
Follow-up time, mean (SD), y	3.50 (4.47)	5.64 (6.53)
Follow-up time, median (Q1–Q3), y	1.67 (0.42–5.00)	3.17 (0.67–8.67)
Birth year, mean (SD), y	1,930 (14.70)	1,940 (18.50)
Age at diagnosis, mean (SD), y	71.00 (11.60)	63.60 (15.10)
Age group (by quantile), no. (%), y		
<55	58,180 (8.48)	1,939,983 (24.79)
55–66	159,108 (23.20)	2,300,439 (29.40)
67–75	206,746 (30.15)	1,827,392 (23.35)
>75	261,693 (38.16)	1,756,895 (22.45)
Calendar year, no. (%)		
1975–1984	26,808 (3.91)	668,993 (8.55)
1985–1994	74,360 (10.84)	988,075 (12.63)
1995–2004	163,161 (23.79)	2,194,895 (28.05)
2005–2016	421,398 (61.45)	3,972,746 (50.77)
Sex, no. (%)		
Male	404,391 (58.97)	4,012,867 (51.28)
Female	281,336 (41.03)	3,811,842 (48.72)
Race, no. (%)		
White	586,494 (85.53)	6,427,454 (82.14)
Black	63,114 (9.20)	797,649 (10.19)
Others/unknown	36,119 (5.27)	599,606 (7.66)
Cohabitation status, no. (%)		
Cohabitation	249,999 (36.46)	2,940,863 (37.58)
Noncohabitation	390,221 (56.91)	4,351,566 (55.61)
Unknown	45,507 (6.64)	532,280 (6.80)
Insurance, no. (%)		
Insured	339,146 (49.46)	3,037,767 (38.82)
Uninsured	3,822 (0.56)	90,885 (1.16)
Unknown	342,759 (49.98)	4,696,057 (60.02)
State, no. (%)		
Alaska	533 (0.08)	7,495 (0.10)
California	216,848 (31.62)	2,767,483 (35.37)
Connecticut	63,227 (9.22)	603,280 (7.71)
Georgia	56,227 (8.20)	733,285 (9.37)
Hawaii	15,738 (2.30)	169,385 (2.16)
Iowa	55,057 (8.03)	508,535 (6.50)
Kentucky	26,320 (3.84)	337,028 (4.31)
Louisiana	23,977 (3.50)	320,179 (4.09)
Michigan	73,514 (10.72)	676,773 (8.65)
New Jersey	52,786 (7.70)	664,090 (8.49)
New Mexico	17,921 (2.61)	223,539 (2.86)
Utah	19,001 (2.77)	220,849 (2.82)
Washington	64,578 (9.42)	592,788 (7.58)
Cancer sites, no. (%)		
Prostate cancer	70,992 (10.35)	1,186,195 (15.16)
Breast cancer	45,939 (6.70)	1,188,792 (15.19)
Colorectal cancer	82,991 (12.10)	835,070 (10.67)
Lung cancer	121,001 (17.65)	975,192 (12.46)
Skin (nonmelanoma)	4,064 (0.59)	28,036 (0.36)
CNS <sup>c</sup> cancer	6,630 (0.97)	113,471 (1.45)
Severe cancer <sup>d</sup>	40,647 (5.93)	388,774 (4.97)
Other cancers	258,521 (37.70)	2,526,393 (32.29)
Smoking-related cancers		
No	434,306 (63.34)	5,814,303 (74.31)
Yes	251,421 (36.66)	2,010,406 (25.69)
Alcohol-related cancers		
No	648,254 (94.54)	7,467,584 (95.44)
Yes	37,473 (5.46)	357,125 (4.56)

TABLE 1: Continued.

	SMN <sup>a</sup> (N = 685727)	FMN <sup>b</sup> (N = 7824709)
Tumor size, no. (%), cm		
<1.5	66,741 (9.73)	791,353 (10.11)
≥1.5	321,740 (46.92)	3,310,859 (42.31)
Unknown	297,246 (43.35)	3,722,497 (47.57)
Tumor grade, no. (%)		
Well differentiated	61,799 (9.01)	734,335 (9.38)
Moderately differentiated	170,021 (24.79)	2,069,948 (26.45)
Poorly differentiated/undifferentiated	155,702 (22.71)	1,900,555 (24.29)
Unknown	298,205 (43.49)	3,119,871 (39.87)
Chemotherapy/radiotherapy		
No/unknown	429,626 (62.65)	4,356,691 (55.68)
Yes	256,101 (37.35)	3,468,018 (44.32)
Surgery		
No/unknown	319,150 (46.54)	3,240,379 (41.41)
Yes	366,577 (53.46)	4,584,330 (58.59)

<sup>a</sup>Second malignant neoplasm. <sup>b</sup>First malignant neoplasm. <sup>c</sup>Central nervous system. <sup>d</sup>Esophageal, liver, or pancreatic cancer.

TABLE 2: Risk of suicide among individuals with a second malignant neoplasm (SMN) diagnosis, by different adjustment strategies, compared with individuals with a first malignant neoplasm (FMN) diagnosis.

Model information	No. of suicide cases/no. of accumulated person-years × 10,000 (incidence rate/10,000 person-years)		Hazard ratio (95% confidence interval)
	SMN	FMN	
Different adjustment strategies <sup>a</sup>			
Model 1: adjusted for birth year, sex, and calendar year			1.24 (1.16–1.32)
Model 2: model 1 + sociodemographic factors (i.e., race, cohabitation status, insurance, and state)			1.23 (1.15–1.32)
Model 3: model 2 + tumor characteristics (i.e., tumor size and tumor grade)	937/2,401,152.92 (3.90)	10930/44,105,958.92 (2.48)	1.22 (1.14–1.31)
Model 4 (full model): model 3 + cancer treatment (i.e., chemotherapy/radiotherapy and surgery)			1.23 (1.14–1.31)

<sup>a</sup>Cox model was used to estimate hazard ratios (HRs), adjusted for covariates listed in the model information column.

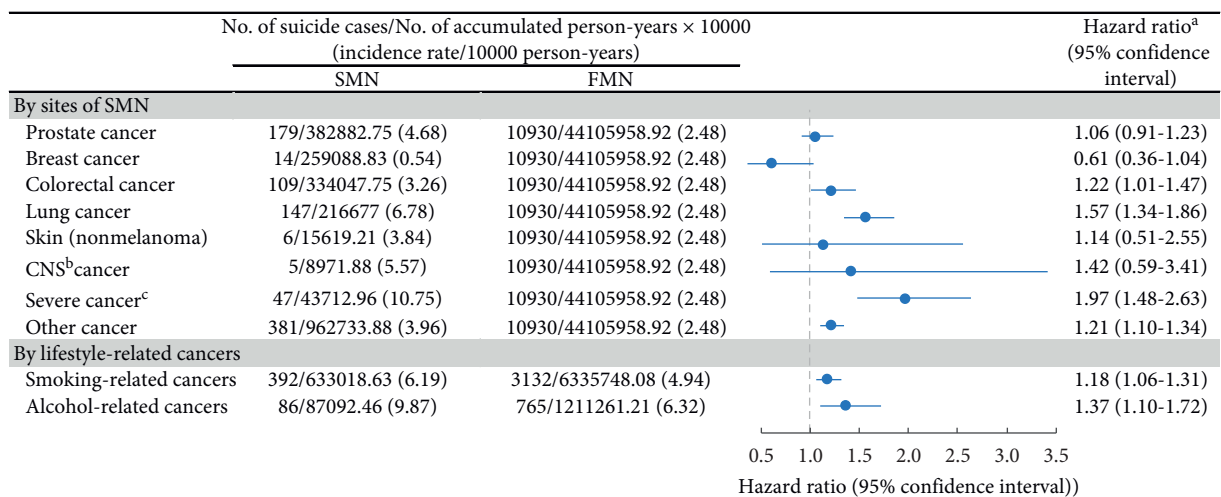


FIGURE 2: Risk of suicide among individuals with a second malignant neoplasm (SMN) diagnosis, by sites of SMN or lifestyle-related cancers, compared with individuals with a first malignant neoplasm (FMN) diagnosis. <sup>a</sup>Cox model was used to estimate hazard ratios (HRs), adjusted for birth year, sex, calendar year, race, cohabitation status, insurance, state, tumor size, grade, chemotherapy/radiotherapy, and surgery. <sup>b</sup>Central nervous system. <sup>c</sup>Esophageal, liver, or pancreatic cancer.

TABLE 3: Risk of suicide among individuals with a second malignant neoplasm (SMN) diagnosis, by different characteristics, compared with individuals with a first malignant neoplasm (FMN) diagnosis.

	No. of suicide cases/no. of accumulated person-years $\times 10,000$ (incidence rate/10,000 person-years)		Hazard ratio <sup>a</sup> (95% confidence interval)	<i>P</i> <sub>difference</sub>
	SMN	FMN		
By age at diagnosis (by quantile), y				0.0003
<55	75/315,337.92 (2.38)	2780/15,810,144.58 (1.76)	1.38 (1.09–1.73)	
55–65	223/687,006.17 (3.25)	3234/13,794,478.21 (2.34)	1.32 (1.15–1.52)	
66–75	339/747,527.17 (4.53)	2816/9,059,181.29 (3.11)	1.33 (1.19–1.50)	
>75	300/651,281.67 (4.61)	2100/5,442,154.83 (3.86)	0.96 (0.85–1.09)	
By calendar year, y				0.15
1975–1984	68/116,017.71 (5.86)	1584/5,375,711.83 (2.95)	1.43 (1.12–1.82)	
1985–1994	191/364,410.29 (5.24)	2296/8,174,559.13 (2.81)	1.40 (1.21–1.63)	
1995–2004	260/789,908.79 (3.29)	3473/16,284,736.13 (2.13)	1.21 (1.06–1.37)	
2005–2016	418/1,130,816.13 (3.70)	3577/14,270,951.83 (2.51)	1.17 (1.05–1.29)	
By sex				0.99
Male	825/1,320,654.54 (6.25)	9030/20,956,633.67 (4.31)	1.20 (1.11–1.29)	
Female	112/1,080,498.38 (1.04)	1900/23,149,325.25 (0.82)	1.20 (0.99–1.46)	
By race				0.066
White	880/2,091,732.79 (4.21)	10060/36,981,749.92 (2.72)	1.23 (1.15–1.32)	
Black	38/181,568.13 (2.09)	368/3,798,398.25 (0.97)	1.70 (1.21–2.41)	
By cohabitation status				0.45
Cohabitation	336/746,244.92 (4.50)	4120/13,911,216.5 (2.96)	1.20 (1.07–1.35)	
Noncohabitation	546/1,493,855.42 (3.65)	5939/27,156,872.79 (2.19)	1.27 (1.16–1.39)	
By tumor size, cm				0.057
<1.5	79/321,027 (2.46)	758/5,869,076.38 (1.29)	1.39 (1.10–1.76)	
$\geq 1.5$	366/1,025,931.79 (3.57)	3640/16,163,041.38 (2.25)	1.08 (0.97–1.21)	
By tumor grade				0.81
Well differentiated	86/306,398.13 (2.81)	1000/5,384,767.58 (1.86)	1.29 (1.03–1.61)	
Moderately differentiated	275/769,611.54 (3.57)	3179/14,044,744.63 (2.26)	1.37 (1.21–1.56)	
Poorly differentiated/ undifferentiated	252/473,608.54 (5.32)	2696/8,978,857.25 (3.00)	1.40 (1.23–1.60)	
By chemotherapy/radiotherapy				0.91
No/unknown	630/1,590,770.13 (3.96)	6701/25,942,336.79 (2.58)	1.22 (1.13–1.33)	
Yes	307/810,382.79 (3.79)	4229/18,163,622.13 (2.33)	1.23 (1.09–1.38)	
By surgery				0.0011
No/unknown	397/662,482.42 (5.99)	4654/10,600,572.79 (4.39)	1.07 (0.96–1.18)	
Yes	540/1,738,670.5 (3.11)	6276/33,505,386.13 (1.87)	1.35 (1.23–1.48)	
By time interval between FMN and SMN, y				0.84
$\leq 1$	246/630,900.92 (3.90)	10930/44,105,958.92 (2.48)	1.24 (1.09–1.40)	
2–3	195/464,630.75 (4.20)	10930/44,105,958.92 (2.48)	1.29 (1.12–1.49)	
4–6	189/486,033.92 (3.89)	10930/44,105,958.92 (2.48)	1.19 (1.03–1.38)	

TABLE 3: Continued.

	No. of suicide cases/no. of accumulated person-years $\times$ 10,000 (incidence rate/10,000 person-years)		Hazard ratio <sup>a</sup> (95% confidence interval)	$P_{\text{difference}}$
	SMN	FMN		
>6	307/819,587.33 (3.75)	10930/44,105,958.92 (2.48)	1.20 (1.07–1.34)	0.95
By follow-up periods, y				
<1	376/509,112.92 (7.39)	3131/6,261,779.63 (5.00)	1.18 (1.06–1.31)	
1–2	153/784,901.33 (1.95)	1510/10,511,420.75 (1.44)	1.26 (1.06–1.49)	
3–4	199/1,328,072.67 (1.50)	2368/20,421,357.75 (1.16)	1.22 (1.06–1.42)	
5–10	143/1,387,784.33 (1.03)	2210/26,923,811.17 (0.82)	1.24 (1.05–1.48)	
>10	66/904,527.5 (0.73)	1711/26,133,082.67 (0.65)	1.28 (1.00–1.63)	

<sup>a</sup>Cox model was used to estimate hazard ratios (HRs), adjusted for birth year, sex, calendar year, race, cohabitation status, insurance, state, tumor size, grade, chemotherapy/radiotherapy, and surgery.

radiotherapy, and the time interval between FMN and SMN (Table 3). Likewise, similar estimates were found across different follow-up periods ( $P_{\text{difference}} = 0.95$ ; Table 3). However, the HRs were somewhat higher among younger patients ( $P_{\text{difference}} = 0.0003$ ) and patients treated with surgery ( $P_{\text{difference}} = 0.0011$ ). A greater risk of suicide was also observed in SMN patients who underwent chemotherapy/radiotherapy ( $P_{\text{difference}} = 0.013$ ) and surgery ( $P_{\text{difference}} = 0.045$ ) for their first malignancy (Table 4).

The calculation of SMRs, using the general US population as a reference, revealed a further increased risk of suicide among SMN patients (SMR 1.65 (95% CI 1.54–1.75)) relative to FMN patients (SMR 1.29 (95% CI 1.26–1.31);  $P_{\text{difference}} < 0.0001$ ). Across different follow-up periods, the changing patterns were similar between SMN patients and FMN patients, both of which showed the highest estimates within the first 3 months after cancer diagnosis (Figure 3 and Supplementary Table 2). The excess risk then experienced a rapid decline but remained at a significant level for up to 5 years.

In sensitivity analysis, we observed largely comparable results after excluding SMN patients whose first malignancy was at the same tumor site (Supplementary Table 3). In addition, the calculation of the  $E$ -value revealed that a minimal magnitude of 1.76-fold increased risk of suicide death that was associated with the unmeasured confounders would be needed to entirely explain the observed association.

#### 4. Discussion

To the best of our knowledge, this is the first large-scale cohort study that examined the risk of suicide among cancer survivors who developed a SMN, using population-based register data in the USA. We found that compared with FMN patients, patients with a SMN diagnosis, particularly those diagnosed at a younger age, with aggressive SMN, or had received surgery treatment for the SMN, were at an increased risk of suicide death within the entire follow-up

period after adjusting for many potential confounders. Importantly, as the calculations of relative risk (i.e., SMR) of suicidal death relative to the general US population revealed a high-risk time period (i.e., the first 3 months after SMN diagnosis), such finding highlights the time window for suicide intervention among SMN patients.

The immediate suicide risk following a FMN diagnosis has been well estimated in previous studies, suggesting cancer diagnosis as an acute stressor that can lead to suicide behaviors [11, 13, 23]. Nevertheless, with regard to SMN, data from large longitudinal studies are scarce. We therefore have limited knowledge about the suicide risk among SMN patients, and whether the level of such a risk is comparable or superior to that among FMN patients. In our study, we, for the first time, showed a significant impact of a SMN diagnosis on the subsequent suicide risk, relative to a FMN diagnosis. Despite the absence of comparable data from studies with a similar design, our findings gain support from previous investigations that consistently suggested cancer survivors with multiple primary cancers had more frequent or greater psychological distress than survivors of single cancer, which was measured by the number of days of self-reported mental-health-related feelings in the past month [15–17]. Such results indicate that a diagnosis of subsequent primary cancer might bring additional adverse effects on the mental health among cancer survivors. Moreover, in a study also based on the SEER database, it focused on the sex disparity of suicide risk among cancer patients, and the authors reported an increased risk for suicidal death among secondary primary head and neck cancer patients, compared with those with head and neck cancer as the first primary cancer, which is in line with our present results [24]. Furthermore, the comparison with the general population corroborates the findings by illustrating consistently higher SMRs among SMN than FMN patients over time since the diagnosis. Those two groups of patients, however, shared a temporal pattern of suicide death risk, with the period shortly after the cancer diagnosis (i.e., within 3 months for both SMN and FMN) as a high-risk time period with the

TABLE 4: Risk of suicide among individuals with a second malignant neoplasm (SMN) diagnosis, by characteristics of the first malignancy, compared with individuals with a first malignant neoplasm (FMN) diagnosis.

	No. of suicide cases/no. of accumulated person-years $\times 10,000$ (incidence rate/10,000 person-years)		Hazard ratio <sup>a</sup> (95% confidence interval)	$P_{\text{difference}}$
	SMN	FMN		
By FMN tumor size, cm				0.57
<1.5	62/260,141.08 (2.38)	758/5,869,076.38 (1.29)	1.55 (0.77–3.12)	
$\geq 1.5$	285/839,718.17 (3.39)	3,640/16,163,041.38 (2.25)	1.26 (1.06–1.50)	
By FMN grade				0.54
Well differentiated	118/318,247.38 (3.71)	1,000/5,384,767.58 (1.86)	1.39 (0.82–2.36)	
Moderately differentiated	334/817,983.33 (4.08)	3,179/14,044,744.63 (2.26)	1.65 (1.37–1.99)	
Poorly differentiated/undifferentiated	212/466,502.54 (4.54)	2,696/8,978,857.25 (3.00)	1.86 (1.47–2.37)	
By FMN chemotherapy/radiotherapy				0.013
No/unknown	590/1,525,397.25 (3.87)	6,701/25,942,336.79 (2.58)	1.28 (1.16–1.41)	
Yes	347/875,755.67 (3.96)	4,229/18,163,622.13 (2.33)	1.64 (1.39–1.95)	
By FMN surgery				0.045
No/unknown	272/512,397.08 (5.31)	4,654/10,600,572.79 (4.39)	1.18 (0.99–1.40)	
Yes	665/1,888,755.83 (3.52)	6,276/33,505,386.13 (1.87)	1.45 (1.31–1.61)	

<sup>a</sup>Cox model was used to estimate hazard ratios (HRs), adjusted for birth year, sex, calendar year, race, cohabitation status, insurance, state, tumor size, grade, chemotherapy/radiotherapy, and surgery.

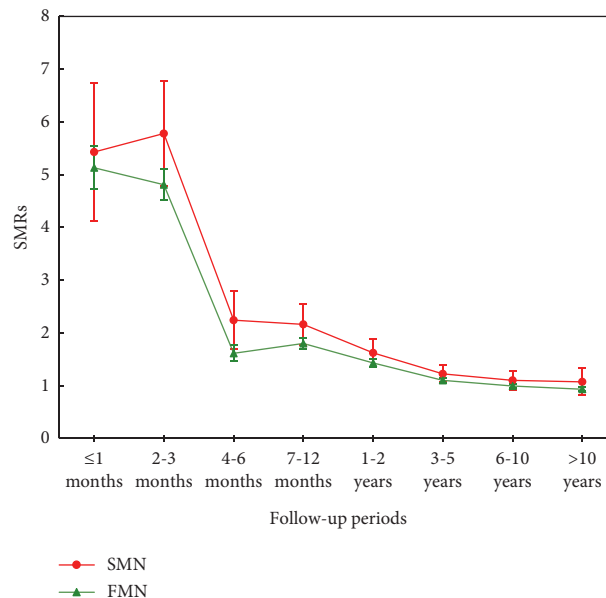


FIGURE 3: Change of the suicide standardized mortality ratios (SMRs) over follow-up periods among patients with first malignant neoplasm (FMN) or second malignant neoplasm (SMN), compared with the general population. The expected number for suicide deaths during the study period was derived from age (5 year groups), sex, and calendar year (1 year groups) suicide death rate for the USA.

most frequent suicide deaths. The observed temporal pattern was in accordance with our previous findings on the risk patterns of mental disorders after the cancer diagnosis [8]. These results further indicate the psychological stress

induced by the diagnosis of the subsequent malignant neoplasm and call for attention to monitor the mental health status of cancer survivors, especially for those who experienced a recent diagnosis of cancer, and to carry out



necessary thought interventions, such as initiating timely psychosocial care [25] and providing prompt suicide risk screening [26].

Besides the repeated exposure to a notorious stressful event such as cancer diagnosis [27], other explanations for the phenomenon that SMN patients might suffer from a higher level of psychological stress, in comparison with FMN patients, include poorer mental health status (e.g., being more likely to have the serious psychological disorder) [15], worse overall health condition (e.g., being reported more health-related bed days) [15], poorer quality of life [28], and undermined socioeconomic status due to the treatment of FMN [29]. In addition, even if patients eventually survived their cancer, cancer treatment itself could be invasive and painful and often accompanied by severe side effects that could traumatize cancer survivors for an extended period of time [30]. Therefore, the fear of cancer treatment can be another underlying trigger that contributes to more suicidal behaviors among SMN patients. Indeed, in our analysis, we found SMN patients who underwent chemotherapy/radiotherapy or surgery for their FMN had a higher relative risk for suicide death, providing supportive evidence to this notion.

The major merits of our study include the large population-based sample of cancer survivors across the USA and the complete follow-up period, which ensures the representativeness of the study sample. Also, the large sample size enabled detailed analyses for all subgroups, especially by different follow-up times since diagnosis. The data on cancer diagnosis and cause of death are collected prospectively and independently, which minimizes the risk of information bias. In addition, using the enriched information on tumor characteristics and cancer treatment, we were able to control for important tumor- and treatment-related confounders in our analysis.

Our study has several limitations. First, the misclassification of some causes of death may be a concern. However, it is unlikely that the misclassification would differ substantially between patients with malignancy and the general population. Second, the SEER program merely recruited cancer patients, lacking a cancer-free group as a reference. However, the comparisons of the suicide rates between our study population and the age-, calendar-year-, and sex-matched general population through SMR calculation facilitate the identification of high-risk time window of suicide for timely and effective intervention. Third, due to the lack of information on some potential confounders, such as lifestyle factors, preexisting psychiatric disorders, and history of somatic illness, the residual confounding could be an issue. During analysis, we have made extra efforts by analyzing lifestyle-related cancers (i.e., alcohol- and smoking-related cancers) separately. As such analyses led to comparable estimates, it seems the lifestyle factor did not substantially modify the observed associations. The role of preexisting psychiatric disorders and history of somatic illness need to be assessed in further investigations. However, the calculated *E*-value suggested that the observed association was

unlikely to be entirely explained by the unmeasured confounding. Finally, the generalization of our findings to the entire nation or other populations needs cautions since SEER areas had better case completeness, greater economic disadvantage, and greater minority diversity than non-SEER areas [31]. Despite these discrepancies, we assume these factors should have a limited effect on the studied association as we compared individuals with FMN to those with SMN in our study, all of which come from SEER areas.

In conclusion, this population-based cohort in the USA indicated that cancer survivors receiving a SMN diagnosis were at an increased risk of suicide, compared with either patients with FMN or the general population. The excess risk was most pronounced within the time period immediately after the SMN diagnosis, highlighting the necessity of providing timely psychological support to patients suffering SMN.

### Data Availability

The data analyzed in this study were obtained from the Surveillance, Epidemiology, and End Results Program (<https://seer.cancer.gov/>).

### Ethical Approval

This study was approved by the Biomedical Research Ethics Committee of West China Hospital (2020.393).

### Disclosure

Part of this work was presented as an oral presentation at the World Congress of Epidemiology on 3–6 September 2021.

### Conflicts of Interest

The authors declare that there are no potential conflicts of interest.

### Authors' Contributions

DL, HS, and HY were responsible for the study's concept and design. YQ did the project management. HY, CW, and JW did the data cleaning and analysis. HY, DL, and HS interpreted the data. HY, DL, and HS drafted the manuscript. YS did the language edits. All the authors approved the final manuscript as submitted and agree to be accountable for all aspects of the work.

### Acknowledgments

The authors acknowledge the efforts of the Surveillance, Epidemiology, and End Results (SEER) Program tumor registries in the creation of the SEER-based database. This work was supported by the National Natural Science Foundation of China (grant no. 81971262 to HS), 1.3.5 project for disciplines of excellence, West China Hospital, Sichuan University (grant no. ZYYC21005 to HS), and

Project Grant from Science and Technology Department of Sichuan Providence (grant no. 2020YFS0575 to HS).

## Supplementary Materials

Supplementary Table 1: International Classification of Disease Oncology (ICD-O) third version codes for diagnoses used in this study. Supplementary Table 2: change of the suicide standardized mortality ratios (SMRs) over follow-up periods among patients with first malignant neoplasm (FMN) or second malignant neoplasm (SMN), compared with the general population. Supplementary Table 3: sensitive analysis of the risk of suicide among individuals with a second malignant neoplasm (SMN) diagnosis, by excluding SMN patients with a prior history of first malignant neoplasm (FMN) at the same tumor site ( $N=40,076$ ), compared with individuals with FMN. (*Supplementary Materials*)

## References

- [1] K. D. Miller, L. Nogueira, A. B. Mariotto et al., “Cancer treatment and survivorship statistics, 2019,” *CA: A Cancer Journal for Clinicians*, vol. 69, no. 5, pp. 363–385, 2019.
- [2] J. Maddams, M. Utley, and H. Møller, “Projections of cancer prevalence in the United Kingdom, 2010–2040,” *British Journal of Cancer*, vol. 107, no. 7, pp. 1195–1202, 2012.
- [3] C. Allemani, T. Matsuda, V. Di Carlo et al., “Global surveillance of trends in cancer survival 2000–14 (CONCORD-3): analysis of individual records for 37 513 025 patients diagnosed with one of 18 cancers from 322 population-based registries in 71 countries,” *Lancet (London, England)*, vol. 391, no. 10125, pp. 1023–1075, 2018.
- [4] Y. Ye, P. Otahal, K. E. Wills, A. L. Neil, and A. J. Venn, “Temporal trends in the risk of second primary cancers among survivors of adult-onset cancers, 1980 through 2013: an Australian population-based study,” *Cancer*, vol. 124, no. 8, pp. 1808–1818, 2018.
- [5] L. B. Travis, S. D. Fosså, S. J. Schonfeld et al., “Second cancers among 40 576 testicular cancer patients: focus on long-term survivors,” *JNCI: Journal of the National Cancer Institute*, vol. 97, no. 18, pp. 1354–1365, 2005.
- [6] N. Donin, C. Filson, A. Drakaki et al., “Risk of second primary malignancies among cancer survivors in the United States, 1992 through 2008,” *Cancer*, vol. 122, no. 19, pp. 3075–3086, 2016.
- [7] A. Pitman, S. Suleman, N. Hyde, and A. Hodgkiss, “Depression and anxiety in patients with cancer,” *BMJ (Clinical Research ed)*, vol. 361, p. 361, 2018.
- [8] D. Lu, T. M. L. Andersson, K. Fall et al., “Clinical diagnosis of mental disorders immediately before and after cancer diagnosis,” *JAMA Oncology*, vol. 2, no. 9, pp. 1188–1196, 2016.
- [9] K. Brasso, S. Ladelund, B. L. Frederiksen, and T. Jørgensen, “Psychological distress following fecal occult blood test in colorectal cancer screening - a population-based study,” *Scandinavian Journal of Gastroenterology*, vol. 45, no. 10, pp. 1211–1216, 2010.
- [10] N. G. Zaorsky, Y. Zhang, L. Tuanquin, S. M. Bluethmann, H. S. Park, and V. M. Chinchilli, “Suicide among cancer patients,” *Nature Communications*, vol. 10, no. 1, p. 207, 2019.
- [11] F. Fang, K. Fall, M. A. Mittleman et al., “Suicide and cardiovascular death after a cancer diagnosis,” *New England Journal of Medicine*, vol. 366, no. 14, pp. 1310–1318, 2012.
- [12] A. M. Saad, M. M. Gad, M. J. Al-Husseini et al., “Suicidal death within a year of a cancer diagnosis: a population-based study,” *Cancer*, vol. 125, no. 6, pp. 972–979, 2019.
- [13] D. Lu, K. Fall, P. Sparén et al., “Suicide and suicide attempt after a cancer diagnosis among young individuals,” *Annals of Oncology*, vol. 24, no. 12, pp. 3112–3117, 2013.
- [14] L. M. Sun, C. L. Lin, W. C. Shen, and C. H. Kao, “Suicide attempts in patients with head and neck cancer in Taiwan,” *Psycho-Oncology*, vol. 29, no. 6, pp. 1026–1035, 2020.
- [15] M. A. Andrykowski, “Physical and mental health status of survivors of multiple cancer diagnoses,” *Cancer*, vol. 118, no. 14, pp. 3645–3653, 2012.
- [16] J. L. Burris and M. A. Andrykowski, “Physical and mental health status and health behaviors of survivors of multiple cancers: a national, population-based study,” *Annals of Behavioral Medicine*, vol. 42, no. 3, pp. 304–312, 2011.
- [17] M. A. Andrykowski and M. M. Goedendorp, “Distress and mental health care and medication use among survivors of multiple primary cancer diagnoses: findings from the 2016 national health interview survey,” *Journal of Psychosomatic Research*, vol. 134, Article ID 110137, 2020.
- [18] D. Lu, L. B. Kenney, L. M. Vrooman, and C. J. Recklitis, “Long-term psychosocial well-being and quality of life among childhood cancer survivors who developed a subsequent malignant neoplasm,” *Journal of Adolescent and Young Adult Oncology*, vol. 10, no. 2, pp. 240–245, 2021.
- [19] N. N. A. Howlader, M. Krapcho, D. Miller et al., Eds., *SEER Cancer Statistics Review. 1975–2016*, 2021, [https://seer.cancer.gov/csr/1975\\_2016/](https://seer.cancer.gov/csr/1975_2016/).
- [20] M. A. Duggan, W. F. Anderson, S. Altekruse, L. Penberthy, and M. E. Sherman, “The surveillance, epidemiology, and end results (SEER) program and pathology,” *American Journal of Surgical Pathology*, vol. 40, no. 12, pp. e94–e102, 2016.
- [21] Q. Shen, D. Lu, M. E. Schelin et al., “Injuries before and after diagnosis of cancer: nationwide register based study,” *BMJ (Clinical Research ed)*, vol. 354, p. 354, 2016.
- [22] T. J. VanderWeele and P. Ding, “Sensitivity analysis in observational research: introducing the E-value,” *Annals of Internal Medicine*, vol. 167, no. 4, pp. 268–274, 2017.
- [23] K. Fall, F. Fang, L. A. Mucci et al., “Immediate risk for cardiovascular events and suicide following a prostate cancer diagnosis: prospective cohort study,” *PLoS Medicine*, vol. 6, no. 12, Article ID e1000197, 2009.
- [24] W. S. Kendal, “Suicide and cancer: a gender-comparative study,” *Annals of Oncology*, vol. 18, no. 2, pp. 381–387, 2007.
- [25] G. Zalsman, K. Hawton, D. Wasserman et al., “Suicide prevention strategies revisited: 10 year systematic review,” *The Lancet PSYCHIATRY*, vol. 3, no. 7, pp. 646–659, 2016.
- [26] B. Gascon, Y. Leung, O. Espin-Garcia, G. Rodin, D. Chu, and M. Li, “Suicide Risk screening and suicide prevention in patients with cancer,” *JNCI Cancer Spectrum*, vol. 5, no. 4, Article ID pkab057, 2021.
- [27] R. S. Mia, “Psychological distress, health behaviors, and benefit finding in survivors of multiple primary cancers: results from the 2010 livestrong survey. oncology nursing forum; 2017,” *Oncology Nursing Society*, vol. 44, pp. 703–711, 2017.
- [28] C. C. Gotay, S. Ransom, and I. S. Pagano, “Quality of life in survivors of multiple primary cancers compared with cancer survivor controls,” *Cancer*, vol. 110, no. 9, pp. 2101–2109, 2007.
- [29] S. M. Belcher, H. S. Donovan, D. H. Bovbjerg, P. R. Sherwood, G. B. Campbell, and S. M. Sereika, “Psychobehavioral risk factors for financial hardship and poor functional outcomes in

- survivors of multiple primary cancers,” *Psycho-Oncology*, vol. 29, no. 3, pp. 507–516, 2020.
- [30] A. L. Stanton, J. H. Rowland, and P. A. Ganz, “Life after diagnosis and treatment of cancer in adulthood: contributions from psychosocial oncology research,” *American Psychologist*, vol. 70, no. 2, pp. 159–174, 2015.
- [31] T.-M. Kuo and L. R. Mobley, “How generalizable are the SEER registries to the cancer populations of the USA?” *Cancer Causes & Control*, vol. 27, no. 9, pp. 1117–1126, 2016.